Lessons from Monte Carlo simulations of the performance of a dual-readout fiber calorimeter

N. Akchurin[a], F. Bedeschi[b], A. Cardini[c], M. Cascella[d], D. De Pedis[g], R. Ferrari[h], S. Fracchia[h], S. Franchino[i], M. Fraternali[j], G. Gaudio[h], P. Genova[j], J. Hauptman[k], L. La Rotonda[l], S. Lee[a], M. Livan[j], E. Meoni[m], D. Pinci[g], A. Policicchio[l], J.G. Saraiva[n], F. Scuri[b], A. Sill[a], T. Venturelli[l], and R. Wigmans[a, 1]

[a] *Texas Tech University, Lubbock (TX), USA*
[b] *INFN Sezione di Pisa, Italy*
[c] *INFN Sezione di Cagliari, Monserrato (CA), Italy*
[d] *Dipartimento di Fisica, Università di Salento, and INFN Sezione di Lecce, Italy*
[g] *INFN Sezione di Roma, Italy*
[h] *INFN Sezione di Pavia, Italy*
[i] *CERN, Genève, Switzerland*
[j] *INFN Sezione di Pavia and Dipartimento di Fisica, Università di Pavia, Italy*
[k] *Iowa State University, Ames (IA), USA*
[l] *Dipartimento di Fisica, Università della Calabria, and INFN Cosenza, Italy*
[m] *Tufts University, Medford (MA), USA*
[n] *LIP, Lisbon, Portugal*

Abstract

The RD52 calorimeter uses the dual-readout principle to detect both electromagnetic and hadronic showers, as well as muons. Scintillation and Čerenkov light provide the two signals which, in combination, allow for superior hadronic performance. In this paper, we report on detailed, GEANT4 based Monte Carlo simulations of the performance of this instrument. The results of these simulations are compared in great detail to measurements that have been carried out and published by the DREAM Collaboration. This comparison makes it possible to understand subtle details of the shower development in this unusual particle detector. It also allows for predictions of the improvement in the performance that may be expected for larger detectors of this type. These studies also revealed some inadequacies in the GEANT4 simulation packages, especially for hadronic showers, but also for the Čerenkov signals from electromagnetic showers.

PACS: 29.40.Ka, 29.40.Mc, 29.40.Vj

Key words: Calorimetry, Čerenkov light, optical fibers, dual readout method

[1] Corresponding author. Email wigmans@ttu.edu, fax (+1) 806 742-1182.

1 Introduction

Dual-readout calorimetry is a novel particle detection technique, which makes it possible to measure electrons, photons and hadrons with very good precision, and without the (inter-)calibration issues that complicate working with traditional calorimeter systems that consist of separate electromagnetic (em) and hadronic sections. There is a growing interest in applying this technique, both for upgrades of existing detector systems (*e.g.,* the CMS experiment at CERN's Large Hadron Collider) and for experiments at proposed future particle colliders or in space.

Generic prototypes of dual-readout calorimeters have been and are being built by the DREAM and RD52 Collaborations. Test results have been published in a number of papers [1]. The largest detector of this type had an instrumented mass of 1350 kg. This was of course more than enough to study em showers (and also muons) in all possible detail. However, high-energy hadron showers are typically only contained at the 90-95% level in an instrument of this size and, therefore, the ultimate performance for hadron detection could not (yet) be assessed properly. However, the results obtained for the incompletely contained showers are very encouraging.

In this paper, we report on an extensive program of Monte Carlo studies of the performance of these unusual particle detectors. The purpose of these studies was:

(1) To test the (limits of the) validity of such simulations with experimental data already obtained. In particular, we were interested in the dependence of the response and the energy resolution on parameters such as the particle's energy and its angle of incidence. The simulations also predicted certain effects that had not yet been studied experimentally, such as the anti-correlation between the two types of signals produced by the calorimeter. Verification of these predictions was also important in assessing the validity of the simulations.
(2) To predict the effects on the performance for certain modifications of the detectors, for example a larger instrumented mass, an increased light yield, or a different choice of absorber medium.

These studies also made us aware of a number of subtle details of shower development and their (observable) consequences in this intricate particle detector. The paper is organized as follows. In Section 2, the structure of the simulated calorimeters and details of the simulation programs are described. Results of the simulations are given in Sections 3, 4 and 5 for muons, electrons and hadrons, respectively. The results are evaluated and discussed in Section 6.

2 Equipment and simulations

The RD52 calorimeters form the second generation of integrated em + hadronic calorimeters based on separate readout of the scintillation and Čerenkov light pro-

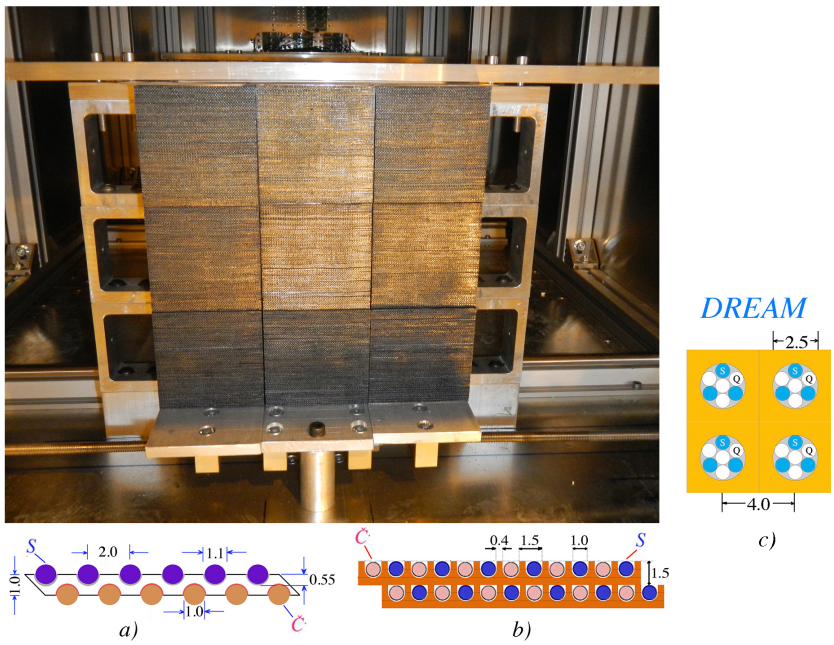

Fig. 1. Front view of the tested SuperDREAM calorimeter, and the basic structure of the lead (a) or copper (b) based modules. For comparison, the structure of the original DREAM calorimeter is shown as well (c). All dimensions are given in mm.

duced in the shower development. Two different types of optical fibers are used as the active media in this detector: Scintillating fibers for the scintillation light and clear PMMA plastic fibers for the Čerenkov light. In the first generation (called DREAM), these two types of fibers were housed together in the holes of extruded copper rods (see Figure 1c). In the RD52 (SuperDREAM) detector, each fiber is separately embedded, which leads to a substantially larger sampling frequency and correspondingly reduced sampling fluctuations. Also, the Čerenkov light is detected in clear plastic fibers, while quartz fibers were used for this purpose in DREAM.

Figure 1 shows a picture of the front face of the RD52 calorimeter. It consists of nine modules, each module is subdivided into four towers, and each tower generates two signals, one from the scintillating fibers and one from the Čerenkov ones. In total, this detector thus produces 72 signals for each event.

These particular modules were built with lead as absorber material. Figure 1a shows a detail of the structure, with alternating layers of scintillating and clear fibers. We also built several modules using copper as absorber material. The fiber arrangement in these modules, depicted in Figure 1b, was slightly different. Each module measured 92×92 mm^2 and contained about 4000 fibers, 2000 of each type.

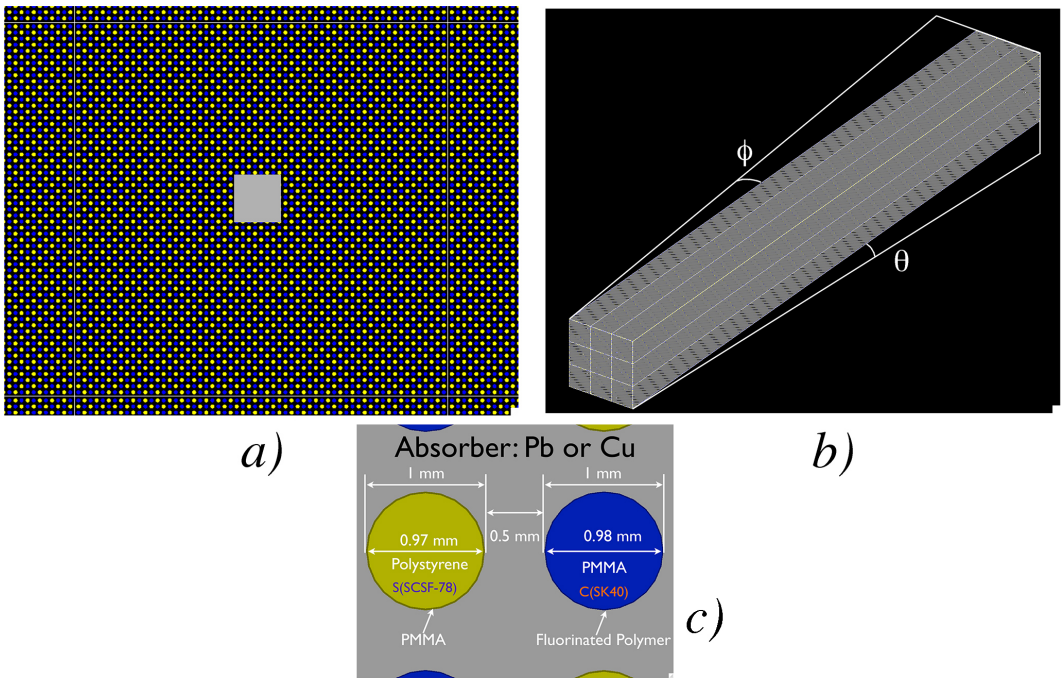

Fig. 2. The simulated calorimeter structure. Shown are part of the front face, including the 10×10 mm^2 beam size used in the simulations (a), the entire calorimeter module oriented at a tilt angle θ and an azimuth angle ϕ with respect to the incident particle beam (b), and a detail of the front face showing the fiber arrangement (c).

2.1 The simulated calorimeter structure

The simulated calorimeter structure was almost identical to the experimental ones. It consisted of nine modules, measuring 92×92 mm^2 each. The fibers were distributed according to a square grid, as shown in Figure 2a,c. Each module contained 3721 fibers. The absorber material could be chosen. In these studies, we used either lead or copper. Small differences with the RD52 calorimeters concerned the fact that no tolerances were applied to the grooves that contain the fibers. Since the simulated modules thus do not contain any air, the sampling fraction is somewhat smaller than for the experimental ones. On the other hand, this is compensated by the fact that light produced anywhere in the 1 mm thick fibers was taken into account in the simulations. In reality, the cladding of the fibers does not contribute to the creation of scintillation light. Also, the fiber arrangement was not exactly the same as in the RD52 calorimeters. In the simulations, a prefectly square grid was used for both types of fibers, while in reality the arrangement was slightly different. Yet, the total number of fibers per module was approximately the same in all cases.

Figure 2b shows the orientation of the entire, 2.5 m long detector, at an angle with respect to the beam particles entering the detector through its front face. The angles θ and ϕ indicate the tilt and the rotation in the horizontal plane, respectively.

All simulations described in this paper were carried out for a calorimeter with the structure described above. However, some of the experimental data with which

comparisons are being made were obtained with the DREAM calorimeter, in which the fiber arrangement was quite different (see Figure 1c). This was true for all muon data, and for the hadron data taken with a copper based calorimeter. In order to assess the possible effects of the different calorimeter structure, a subset of the simulations was **also** performed for a calorimeter structure that closely represented the one shown in Figure 1c. The results of this exercise are described in the appendix [2] . In the same spirit, we have also investigated the possible effects of air gaps inside the calorimeter structure, and the effects of changing the physics list in the simulations. The results of this work are also decribed in the appendix. The figures shown in the following sections were obtained for the calorimeter structure from Figure 2, unless explicitly stated otherwise.

2.2 The simulations

The simulations were carried out with the GEANT4 Monte Carlo package [2]. Events were generated with GEANT4.9.6 patch-02, which was released in May 2013. For applications of calorimetry in high energy physics, GEANT4 recommends to use the FTFP_BERT physics list which contains the Fritiof model [3], coupled to the Bertini-style cascade model [4] and all standard electromagnetic processes. This is the default physics list used in simulations for the CMS and ATLAS experiments at CERN's Large Hadron Collider [5].

Each run consisted of typically 3000 events. The impact point of the particles was randomly distributed over a 10×10 mm^2 area around the center of the detector. For the (highly directional) Čerenkov light, each photon was examined and followed all the way as it propagated to the rear end of the detector if it was emitted within the numerical aperture of the fiber. In order to translate the Čerenkov signals into a measured number of photoelectrons, an overall quantum efficiency factor was applied [3] . This quantum efficiency depends on a number of factors that change from photon to photon: The photon energy, the angle of incidence, the point of incidence on the photocathode, *etc.* This is impossible to simulate. For that reason, we have chosen to used a fixed number for this quantum efficiency throughout these simulations: 0.11. This number is very reasonable, since it reproduces the "light yield" (*i.e.,* the average number of photoelectrons produced per GeV deposited energy, which we measured in several different ways) quite well. Any other choice of this quantum efficiency would *only* have affected the em energy resolution, which is dominated by Poisson fluctuations in the number of photoelectrons, but *none* of the other characteristics of the Čerenkov signals discussed in this paper.

[2] Since experimental muon data were *only* obtained with the DREAM calorimeter, the experimental results are in this case compared with the results of these additional simulations in the text (Section 3).

[3] We used the Optical Boundary (OpBoundary) process provided in GEANT for this purpose.

The numerical aperture was calculated on the basis of the indices of refraction provided by the producers of the fibers used in the calorimeters: $n = 1.49$ and 1.42 for the core and cladding materials of the PMMA fibers, $n = 1.458$ and 1.42 for the core and cladding materials of the quartz fibers used in the DREAM calorimeter.

For the scintillation signals, it was not necessary to follow each photon in detail. Since the scintillation photons are emitted isotropically, the signals were (in first approximation) proportional to the energy deposited in the scintillating fibers by the ionizing shower particles. However, there is one important caveat: Saturation of the light produced by densely ionizing particles. This phenomenon especially affects the hadronic scintillation signals, in particular the contributions from protons produced in nuclear breakup and neutron scattering. It is described by the following expression:

$$\frac{dL}{dx} \propto \frac{dE/dx}{1 + k_{\mathrm{B}} \cdot dE/dx} \tag{1}$$

where L is the amount of light produced by a particle of energy E and k_{B} a material property known as Birks' constant [6]. This constant is typically of the order of 0.01 g cm^{-2} MeV^{-1}, whereas the specific ionization (dE/dx) of a minimum ionizing particle *mip* is of the order of 1 MeV g^{-1} cm^2. In comparison with *mip*s, the specific light production (photons per unit energy) is thus reduced by a factor 2 (11) for particles with a specific ionization of 100 (1000) times the value for minimum ionizing particles. For the scintillating fibers used in our calorimeters, k_{B} was determined to be 0.126 mm/MeV [7], and this is the value we used to convert deposited energy into scintillation signals in these simulations.

2.3 Calibration

Just like in the analyses of all the experimental data obtained with the DREAM and RD52 dual-readout calorimeters, the energy scale in our simulations was determined from the response to 40 GeV electrons, both for the scintillation and the Čerenkov signals. The angle of incidence of the beam particles was the same for the calibration and for the electron energy scan, both in the experiment and in the simulations: $(\theta, \phi) = (1.0^\circ, 1.5^\circ)$. Electrons entering a tower in its center deposit typically about 85% of their energy in that tower, regardless of their energy. The establishment of the relationship between deposited energy and the average resulting signal (*i.e.,* the calibration constants) is thus straightforward when electrons are being sent into each calorimeter tower. These calibration constants were subsequently used to determine the energy equivalence of the signals recorded for all other particles (electrons, hadrons and muons).

In the analyses of the experimental data, corrections had to be applied for light at-

tenuation in the fibers [8,9]. This was necessary in order to convert the signals from hadrons and muons, which produce light much deeper inside the calorimeter than the electrons that were used for the calibration, to the same energy scale. However, in the simulations this procedure was not necessary, since the signals from these particles are automatically converted to that energy scale by using the calibration constants as derived above. On the other hand, light attenuation corrections in the simulations would be needed if one wanted to compare with raw experimental signal distributions.

3 Results for Muons

Detailed experimental studies of the muon response functions were only carried out with the original DREAM calorimeter [9]. In order to avoid contributions from signals generated in the windows of the PMTs, these studies were performed at an angle of incidence (θ, ϕ) of (0.7°,6°).

The simulations were performed both with the standard (RD52) geometry, and with the actual (DREAM) geometry in which the experimental data were obtained. In Figure 3, the latter simulation results are shown, together with the experimental data [4].

The most interesting experimental result of the muon studies is the fact that the deposited energy, as derived from the observed signals, is not the same for the two types of fibers. As the muon energy increases from 40 to 200 GeV, the average measured energy loss increases substantially, as a result of the increased bremsstrahlung losses. However, the energy loss measured with the scintillating fibers is systematically larger than for the clear ones, by a constant amount. The explanation of this remarkable fact is that the clear fibers do not produce a signal from the ionization component of the energy loss, since the Čerenkov photons emitted in that process fall outside the numerical aperture of the fibers. The clear fibers thus only register the muon's radiation losses, while the scintillating fibers *in addition* also detect the ionization loss.

The results of the GEANT4 simulations, shown in Figure 3, also exhibit a systematic and constant difference between the muon's energy loss derived from the signals in the two types of fibers. However, this difference is somewhat smaller than in reality, mainly because the simulated Čerenkov signals are a bit larger than the measured values. This is also illustrated in Figure 4, where the ratio of the average scintillation and Čerenkov signals is plotted as a function of the muon energy. Just as in the experimental data, the simulated ratio increases with energy, but the value of that ratio is about 20-25% larger than in practice.

[4] The simulations with the RD52 geometry confirmed the conclusions described in this section. See appendix for details.

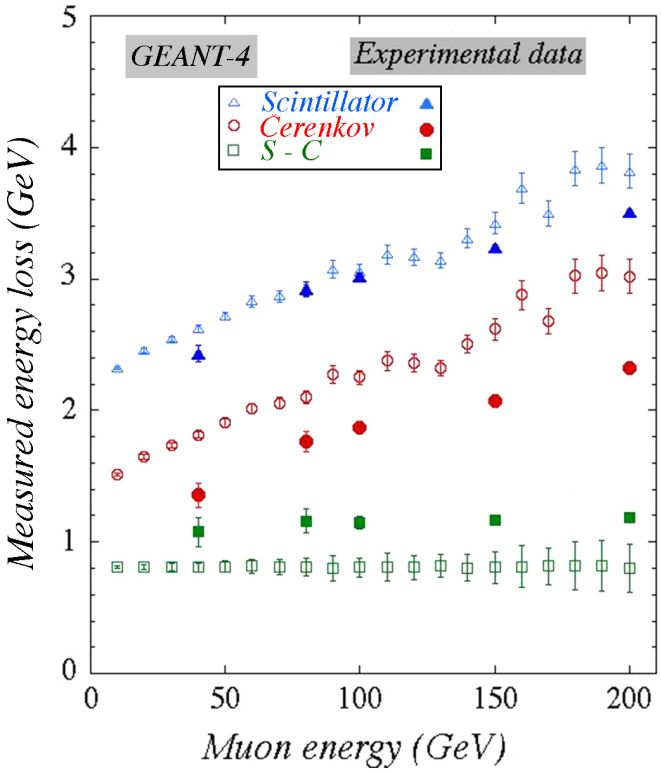

Fig. 3. The average measured energy loss by muons in the DREAM copper calorimeter, as a function of the muon energy. The experimentally measured results are compared with the GEANT4 simulated ones. The DREAM calorimeter was calibrated with 40 GeV electrons. The simulations were performed for the actual (DREAM) structure of the calorimeter with which the experimental data were obtained (Figure 1c).

4 Results for Electrons

4.1 The e/mip ratio

An important characteristic of any sampling calorimeter is the so-called e/mip ratio. This parameter indicates the efficiency with which electromagnetic showers are sampled, relative to minimum ionizing particles. As we will see, this parameter depends on the choice of the absorber material and has profound consequences for some aspects of the calorimeter performance.

The efficiency with which *mip*s are sampled follows directly from the structure of the calorimeter, and the materials of which it is composed. In our case, the cross section of one simulated module measures $92\times92 = 8464$ mm^2. It contains 3721 round fibers with a diameter of 1 mm each, for a total cross section of 2922 mm^2, 1461 mm^2 for each of the two types of fibers. The remaining 5542 mm^2 is taken by the absorber material, since no air gaps around the fibers are assumed.

The specific energy loss of a *mip* amounts to 12.73 MeV/cm in lead, *vs.* 12.57 MeV/cm for copper. For the fibers, the specific energy loss is 2.05 MeV/cm for

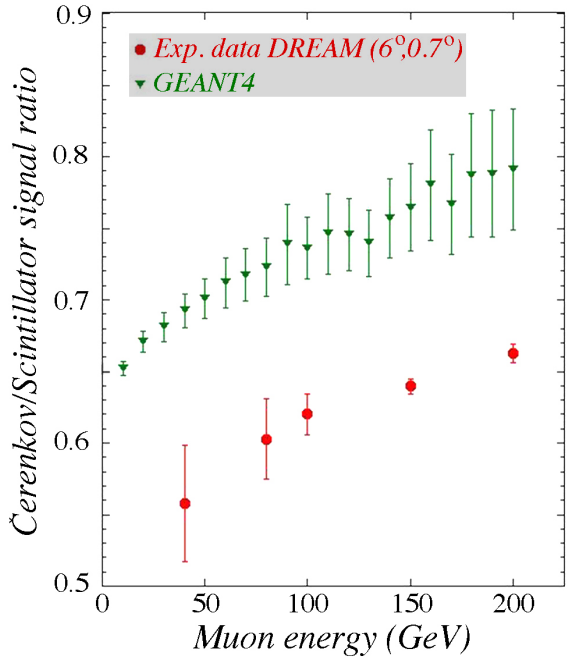

Fig. 4. The ratio of the average Čerenkov and scintillation signals from muons traversing the calorimeter, as a function of the muon energy. The experimentally measured results [9] are compared with the GEANT4 simulated ones. The calorimeters were calibrated with 40 GeV electrons, and the simulations were performed for the actual (DREAM) structure of the calorimeter with which the experimental data were obtained (Figure 1c).

the (polystyrene) scintillating fibers, and 2.30 MeV/cm for the (PMMA) Čerenkov ones. This leads to a sampling fraction for *mip*s of $(2.05 \times 1461)/(2.05 \times 1461 + 2.30 \times 1461 + 12.57 \times 5542) = 3.94\%$ for the copper/scintillating-fiber structure and 3.89% for the lead/scintillating-fiber one.

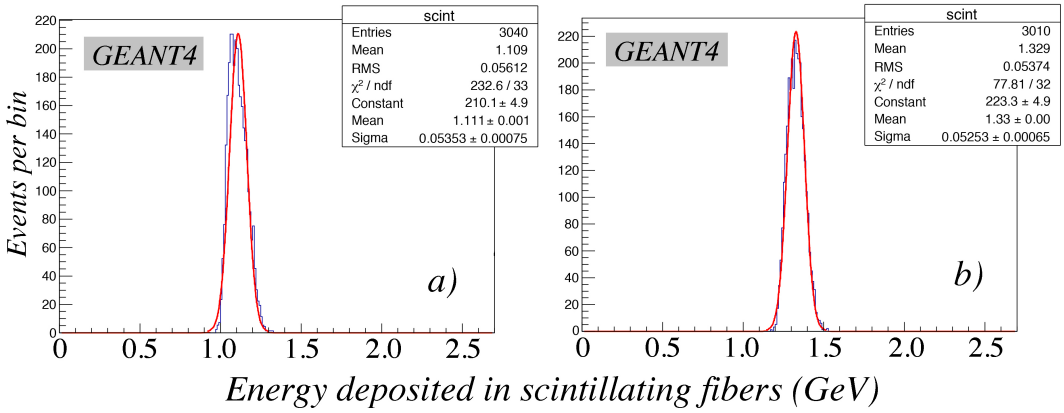

Fig. 5. Distribution of the energy deposited by 40 GeV electrons in the scintillating fibers of the lead (a) and the copper (b) calorimeter structure. The angle of incidence of the electrons (θ, ϕ) was (1.0°,1.5°) in these GEANT4 simulations.

As is shown later in this section, the sampling fraction for electromagnetic showers is, for all practical purposes, independent of the energy and the angle of incidence

of the electrons. Figure 5 shows representative scintillation response functions, for 40 GeV electrons in the lead (Figure 5a) and copper (Figure 5b) modules, respectively. On average, these electrons deposit 1.109 and 1.329 GeV in the scintillating fibers and, therefore, the sampling fractions for the em showers in these calorimeters amount to 2.77% (lead) and 3.32% (copper), respectively. And thus we find that the e/mip ratios are 0.71 for the lead/scintillating-fiber calorimeter and 0.84 for the copper/scintillating-fiber one.

In the early days of calorimetry, it was generally believed that in an em shower, the energy is deposited by a large collection of minimum ionizing particles (electrons and positrons), and that therefore the e/mip ratio has to be 1.0. The fact that this was not the case in practice gave rise to a lot of speculations [10–12]. However, the explanation for this phenomenon turned out to be the fact that a large fraction of the shower energy is deposited in the late stages of the shower development, through processes such as Compton scattering and the photoelectric effect. In a sampling calorimeter, the energy sharing between the different materials is for these processes very different than for minimum ionizing particles traversing the calorimeter. For example, the cross section for photoelectric effect is proportional to Z^5. This means that in a lead/plastic structure, photoelectrons are in practice only produced in the absorber, and these photoelectrons only contribute to the signal if they are produced sufficiently close to the boundary with a plastic fiber. In practice, the response to the particles produced in the late stages of the shower development is thus suppressed compared to the response to *mip*s. This suppression is larger in calorimeters with high-Z absorber material and in calorimeters with a small sampling frequency (*i.e.,* thick absorber layers) [13].

Just like in the early days of EGS3 [14], the Monte Carlo simulations confirm the essential aspects of this explanation. The suppression of the late-stage signals is clearly more important when lead ($Z = 82$) is used as absorber than for copper ($Z = 29$). Yet, the suppression is somewhat less in this fine-sampling structure than in more crudely sampling lead/plastic-scintillator calorimeters such as the one built by members of the ZEUS Collaboration, for which an e/mip value of 0.67 was reported [15].

One consequence of these results is that the calorimeter signal of the lead calorimeter is more strongly dominated by the early, highly collimated shower component than that of the copper calorimeter. In the latter, the diffuse rather wide component from particles generated beyond the shower maximum plays a larger role. The effects of this difference manifest themselves, for example, in the quality of a Gaussian fit to the response function. Figure 5 shows that the (normalized) χ^2 of this Gaussian fit amounts to 233/33 for lead and 77.8/32 for copper. The explanation of this difference is the topic of the next subsection.

4.2 The calorimeter response function for electrons

4.2.1 Angular dependence of the scintillator response functions

The lateral profile of em showers has several components. Before the shower maximum, the energy is primarily deposited by energetic e^+e^- pairs that travel in almost the same direction as the incoming primary electron. Beyond the shower maximum, electrons from processes such as Compton scattering have a very different, much broader angular distribution. The RD52 Collaboration has measured the lateral shower profile for 100 GeV electrons [16], which shows that $\sim 20\%$ of the shower energy is deposited in an area of 2×2 mm^2 around the shower axis. Since the early, collimated shower component is extremely narrow, the calorimeter response becomes dependent on the impact point of the electrons when these particles travel in the same direction as the fibers. An impact point in a scintillating fiber will lead to a larger scintillation signal than an impact point somewhere in between scintillating fibers, *i.e.,* in the absorber material or a Čerenkov fiber. This is because the early, collimated component generates a large signal contribution in that one hit fiber.

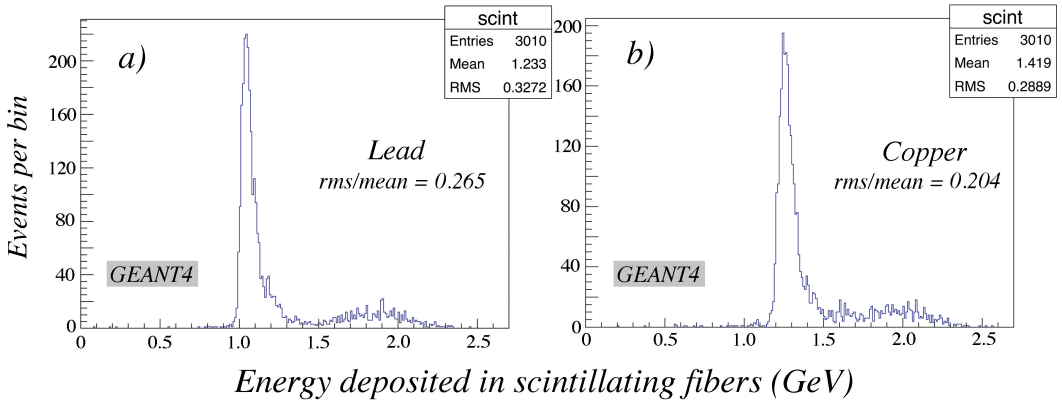

Fig. 6. Distribution of the energy deposited by 40 GeV electrons in the scintillating fibers of the lead (a) and the copper (b) calorimeter structure. The angle of incidence of the electrons (θ, ϕ) was (0°,0°) in these GEANT4 simulations.

Figure 6 shows the effect of this. The response function for 40 GeV electrons consists of two distinctly different components. The broad component represents the events in which the beam particles entered the calorimeter in a scintillating fiber. The signals are in this case larger than those constituting the narrow component, which contains all the other events. It is interesting to compare the response functions for the lead (Figure 6a) and copper (Figure 6b) calorimeters in some detail. Both exhibit the same double-hump structure, but the difference between the mean response values of these two humps is clearly smaller in the case of copper.

This can, for example, be concluded from the value of the ratio *rms/mean* for these distributions: 0.265 for lead, 0.204 for copper. The reason for this difference is the same as the reason for the difference in e/mip values, discussed in the previous subsection. The larger the relative contribution of the late, broad shower component

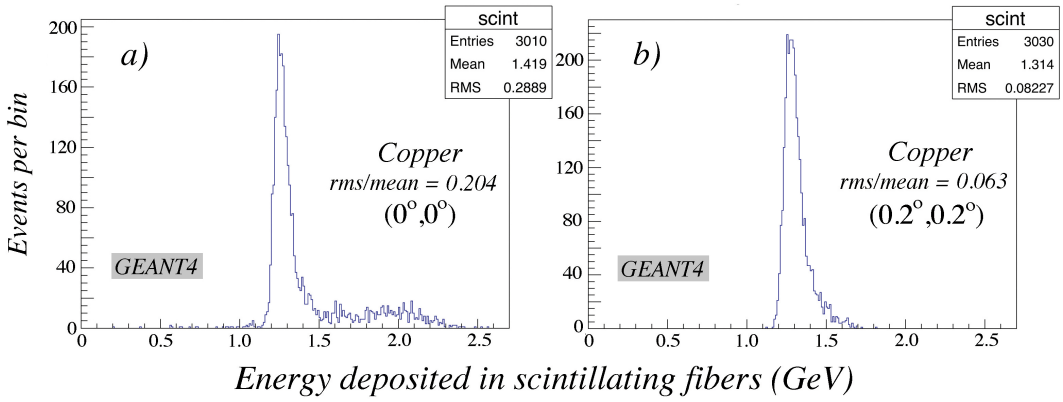

Fig. 7. Distribution of the energy deposited by 40 GeV electrons in the scintillating fibers of the copper calorimeter structure. The angle of incidence of the electrons (θ, ϕ) was (0°,0°) in diagram a and (0.2°,0.2°) in diagram b. Results from GEANT4 simulations.

to the calorimeter signal, the smaller the difference between the mean signals from events where the electron enters the calorimeter in a scintillating fiber or elsewhere, *i.e.,* the smaller the *rms/mean* value for the total signal distribution.

The extreme sensitivity of the calorimeter response to the impact point of the showering electrons exhibited in Figure 6 rapidly decreases when the electrons enter the calorimeter at a small angle with the fiber direction. In that case, the early, collimated shower component does not entirely develop inside a single fiber, but is increasingly sampled just like the shower particles produced in the later stages. Since the fibers have a radius of only 0.5 mm, and the radiation length of the copper calorimeter (which sets the scale for the longitudinal shower development) is about 50 times larger, the angle of incidence for which this becomes a significant effect is very small indeed.

This is illustrated in Figure 7, which shows the effect of rotating the angle of incidence (θ, ϕ) from (0,0) to $(0.2°, 0.2°)$ on the response function of the scintillation signals from the copper calorimeter. The high-side tail of the response function almost completely disappears as a result of this very small rotation. In this process, which corresponds to tilting and displacing the rear end of the calorimeter module by only 6 mm, the *rms/mean* value of the scintillator response function is reduced from 0.204 to 0.063. In fact, the orientation of the calorimeter is so senstive to the precise value of (θ, ϕ), that in practice extreme response functions such as those displayed in Figure 6 have never been observed in our measurements [5] . Yet, the fact

[5] It should be pointed out that the angular divergence of the beam particles played no role in this. This divergence was smaller than 0.1 mrad, *i.e.,* more than a factor of 30 smaller than the effect of a rotation from 0 to 0.2°. The fact that extreme response functions such as the one shown in Figure 7a have not been observed in practice is more likely due to the difficulty of precisely orienting the module with respect to the beam line. It may also be a consequence of the fact that the fibers are never perfectly straight, for example because of tolerances in the grooves that contain them.

that the em response function of fiber calorimeters substantially broadens when the angle between the incident particles and the fiber direction approaches zero is experimentally well established [17].

As illustrated by Figure 5, further rotation to angles of the order of 1° leads to a complete disappearance of the high side tail. Only the relatively poor χ^2 of the Gaussian fit, especially for the lead calorimeter, is testimony to the effects that spoil the scintillator response function for angles of incidence very close to zero. The differences between the lead and copper structures can be understood from the fact that the radiation length of lead is almost a factor of three smaller than for copper. As a result, the extremely collimated part of the shower extends much less in depth, and a small rotation of the calorimeter has a correspondingly smaller effect on the energy sharing of this component between the active and passive calorimeter media.

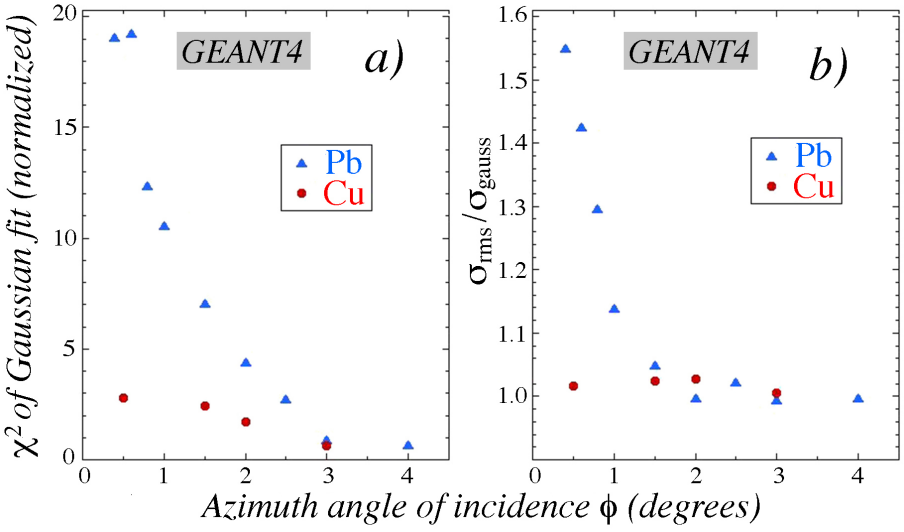

Fig. 8. The normalized χ^2 of a Gaussian fit (χ^2/ndf) to the response function (a) and the ratio of the rms width and the σ of a Gaussian fit (b) as a function of the azimuth angle of incidence ϕ of the 40 GeV electrons. The tilt angle θ was chosen to be 1° in all simulations. Results are given separately for these GEANT4 simulations of em shower development in the lead and copper/scintillating-fiber structures.

Figure 8 shows how the quality of a Gaussian fit to the scintillator response function improves as the angle is increased. Results are given separately for the lead and copper structures. When the angle θ reaches values of 2-3°, the response function is in very good approximation Gaussian, even for lead.

4.2.2 Comparison of the scintillator and Čerenkov response functions

We now turn our attention to the Čerenkov response function. Experimentally, we have observed that the deviations from a Gaussian shape that characterize the scintillator response function for very small angles of incidence are practically absent

for the Čerenkov signals [16,8], especially in copper. The Monte Carlo simulations confirmed this phenomenon, as illustrated in Figure 9, which shows the simulated response functions for 40 GeV electrons in the scintillation and Čerenkov channels for a lead calorimeter oriented at (1°,1°) and a copper one oriented at (0.4°,0.4°).

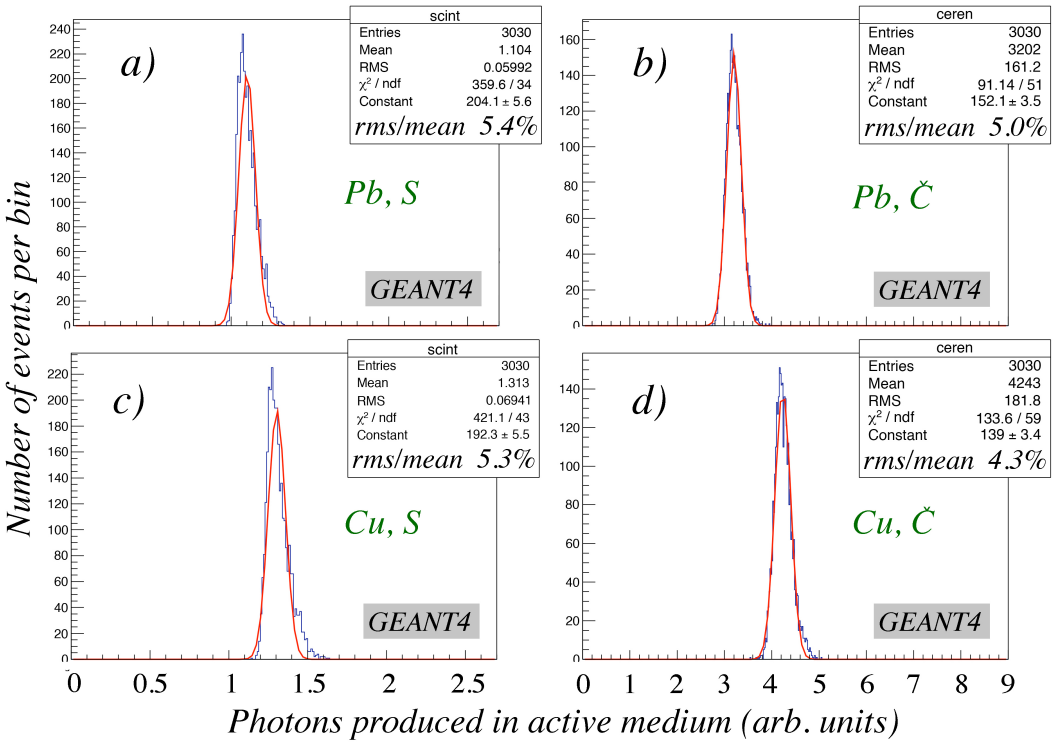

Fig. 9. Comparison of the response functions to 40 GeV electrons for the scintillator (a, c) and Čerenkov (b, d) channels in the lead (top row) and copper (bottom row) calorimeter structures. The angle of incidence (θ, ϕ) in these GEANT4 simulations was $(1.0°, 1.0°)$ in lead and $(0.4°, 0.4°)$ in copper. These values were chosen because of the substantial differences between the quality of Gaussian fits to the scintillation and Čerenkov response functions at these angles.

This effect can be quantified by means of variables that measure the quality of a Gaussian fit to the data points, such as the normalized value of the χ^2, or the ratio of the rms width of the signal distribution and the σ of a Gaussian fit. In Figure 10, the values of these variables are plotted as a function of the azimuth angle of incidence for the scintillation and Čerenkov signals from the lead calorimeter.

They clearly show to what extent the Čerenkov response function is better described by a Gaussian fit than the response function measured with the scintillation signals.

The reason for these differences is the fact that the photons produced in the extremely collimated early shower component do not contribute to the Čerenkov signals. Since these photons are emitted at an angle of about 50° with the direction of the shower axis (and thus with the fibers), they fall ouside the numerical aperture of the fibers. This is essentially the same reason why light produced by the ionization

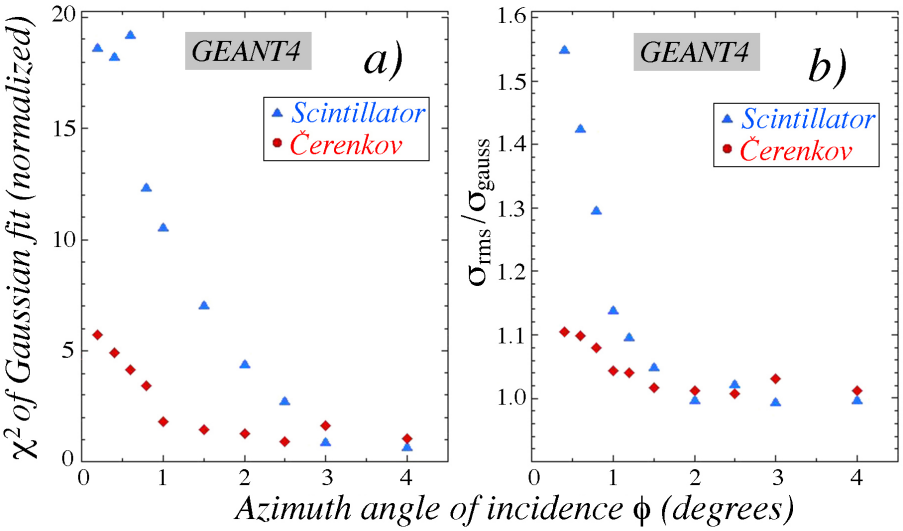

Fig. 10. The χ^2 of a Gaussian fit to the response function (a) and the ratio of the rms width and the σ of a Gaussian fit (b) as a function of the azimuth angle of incidence ϕ of the 40 GeV electrons. The tilt angle θ was chosen to be 1° in all these GEANT4 simulations. Results are given separately for the scintillation and Čerenkov signals in the lead structure.

component does not contribute to the muon Čerenkov signals (see Section 3). As a result, the Čerenkov signals have a somewhat broader radial shower profile than the scintillation signals and, therefore, the response is less dependent on the impact point of the particles.

Effects similar to those depicted in Figure 10 were observed for the copper structure. However, since the angular dependence of the response functions is considerably smaller than for lead to begin with, the differences between the response functions for the two types of fibers is less spectacular than in lead.

4.3 Response, signal linearity and shower containment

In the practice of particle physics experiments, a very important characteristic of a calorimeter is the precision with which one can measure the energy of particles developing showers in it. This precision is usually assessed by measuring the energy resolution for beams of mono-energetic particles entering the detector in a precisely known point and along a precisely known line. In this subsection, we discuss some other aspects of this problem.

In this paper, we define the *response* of a calorimeter as the average signal per unit energy. A calorimeter is said to be *linear* if the signals it produces are proportional to the energy of the absorbed particles, in other words if the *response is constant.* We simulated the development of electrons of different energies, entering the calorimeter at different incident angles to investigate these issues.

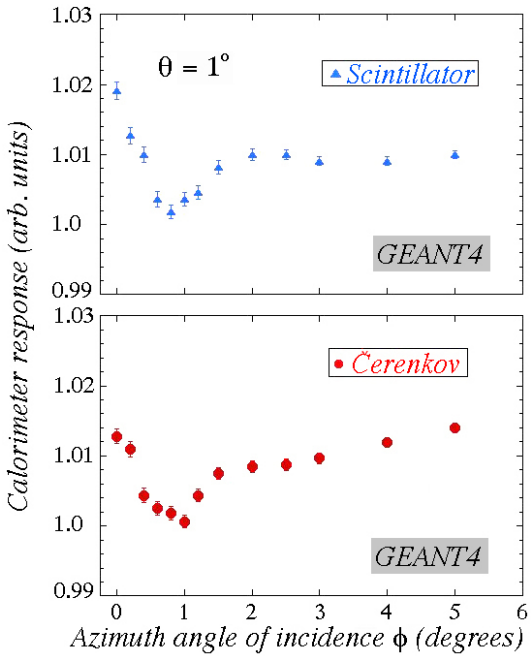

Fig. 11. Angular dependence of the electromagnetic calorimeter response for lead. Shown are the average scintillation (a) and Čerenkov (b) signals per GeV deposited energy as a function of the azimuth angle of incidence ϕ. The tilt angle was 1° in these simulations.

Figure 11 shows the angular dependence of the response to electrons developing showers in the lead calorimeter. These results were obtained at 40 GeV, but the results at other energies were not significantly different. The tilt angle θ was chosen to be 1° in these simulations, and that did affect the results. The dip at $\phi = 1°$ is a consequence of the fiber arrangement in the simulated structure. As can be seen in Figure 2c, particles entering the detector at angles $\phi = \theta$ (*e.g.,* 1°,1°) can travel through a very narrow corridor without encountering any fiber. We verified that this effect also occurs for other geometries in which the angles of incidence in the horizontal and vertical planes were the same ($\phi = \theta$). In each case, the ϕ dependence of the response exhibited a $\sim 1\%$ dip in the vicinity of the tilt angle (θ). No such effects were observed at any other angle of incidence. The increased response at $\phi = 0$ is a consequence of the impact point dependence discussed in the previous subsection (see for example Figure 7). Figure 11 shows that for angles $\phi > 1°$, the response is constant to within $\pm 0.5\%$, at least for the scintillation signals. The Čerenkov response increases very slightly with the angle of incidence, by $\sim 1\%$ between $\phi = 1°$ and 5°. This is a consequence of the directionality of the Čerenkov light. As the angle of incidence increases, the acceptance of light emitted by the shower particles in the fibers gradually increases, to reach a maximum at the Čerenkov angle of 51° [16].

The linearity of the calorimeter was determined from simulations of electrons entering it at an angle of (1.0°,1.5°), which corresponds to the orientation used in most of our beam tests. Results are shown in Figure 12, and indicate linearity to within $\pm 0.5\%$, for electrons in the energy range from 5 - 150 GeV. Experimental

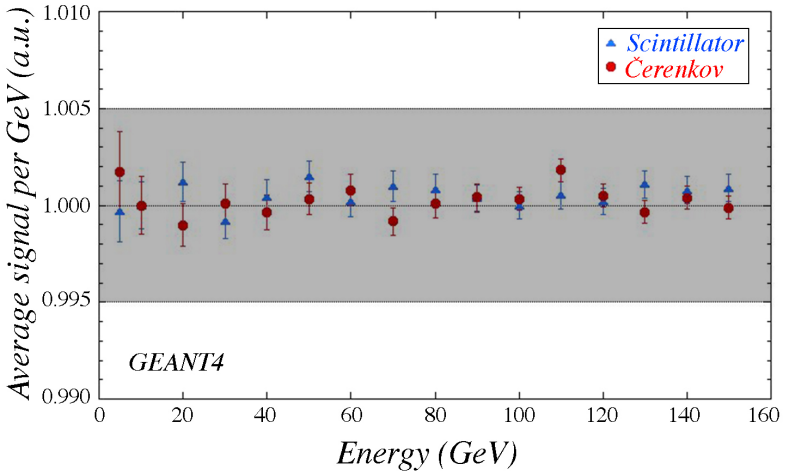

Fig. 12. The linearity of the simulated (copper) calorimeter, for electrons at an incident angle of (1.0°,1.5°). The shaded area represents a constant response to within $\pm 0.5\%$.

measurements have shown that the em response of the RD52 calorimeter was linear to within $\pm 1\%$ over the energy range 10 - 150 GeV [16].

Simulations of the energy deposit profile made it possible to determine the energy fraction contained in one of our RD52 calorimeter towers or modules (see Figures 1,2). For 100 GeV electrons, entering the detector along the fiber direction (*i.e.,* angle of incidence 0,0) in the geometrical center, the simulations gave a containment of 87% in one tower and 96% in one 4-tower module. These numbers are consistent with those measured experimentally (*e.g.,* 85% containment in one tower for particles entering at (1.0°,1.5°) in a 10x10 mm^2 squared area around the tower center [16]).

4.4 The em energy resolution

4.4.1 Angular dependence of the em energy resolution

The small-angle effects on the em response function discussed in subsection 4.2 also have important consequences for the electromagnetic energy resolution of this type of calorimeter. This em energy resolution is affected by Poisson fluctuations in the sampled energy fraction and in the number of photoelectrons. If this were all, one would expect the resolution to be better for the scintillation signals than for the Čerenkov ones. This is because the sampling structure is exactly the same for the two types of fibers, while the light yield for the scintillation process is much larger than for the Čerenkov effect. Yet, as illustrated by Figure 9, for small incidence angles the resolution is clearly better for the Čerenkov signals, especially in the case of the copper calorimeter.

Figure 13 shows the em energy resolution in the lead calorimeter as a function of the azimuth angle of incidence. For angles $\phi > 2°$, the resolution is better for the

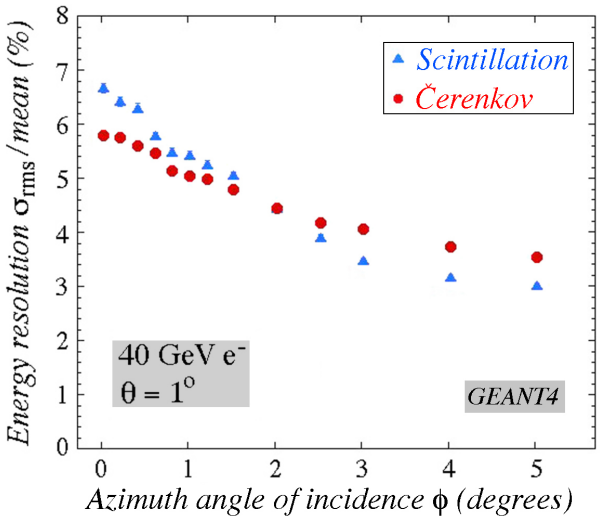

Fig. 13. The dependence of the energy resolution on the azimuth angle of incidence ϕ. Results for 40 GeV electrons in the lead calorimeter structure. The tilt angle θ was 1° in these simulations.

scintillation signals, but for smaller angles the Čerenkov signals provide a better resolution.

These phenomena have the same origin as the differences observed between the Čerenkov and scintillation response functions (see Figure 10). At small angles of incidence, the scintillation response depends much more on the impact point than the Čerenkov response. This dependence on the impact point of the particles is responsible for an additional contribution to the energy resolution. This contribution is in first approximation independent of the electron energy and thus leads to a constant term in the energy resolution. The Poisson fluctuations in the sampled energy fraction and the light yield each contribute a term that scales as $E^{-1/2}$ to the energy resolution and, therefore, the effects of the impact point dependence are most prominently visible at high energy.

Figure 14 shows the energy resolution in the copper calorimeter for electrons at an incident angle of (1.0°,1.5°). The simulations were carried out for electron energies of 5 GeV and from 10 - 150 GeV in steps of 10 GeV. The results are represented by the curves drawn in Figure 14: A solid (blue) line for the scintillation signals, a dashed (red) line for the Čerenkov signals and a dotted (green) line for the sum of both signals. The figure also contains the experimental resolutions, measured with the RD52 copper calorimeter [16].

The Čerenkov resolution was obtained using a quantum efficiency factor of 0.11, which corresponds to a light yield of $\sim$ 30 Čerenkov photoelectrons per GeV deposited energy, in good agreement with measured values for this light yield [16]. The figure also shows good agreement between the simulatied and measured em energy resolutions, both for the scintillation and the Čerenkov signals.

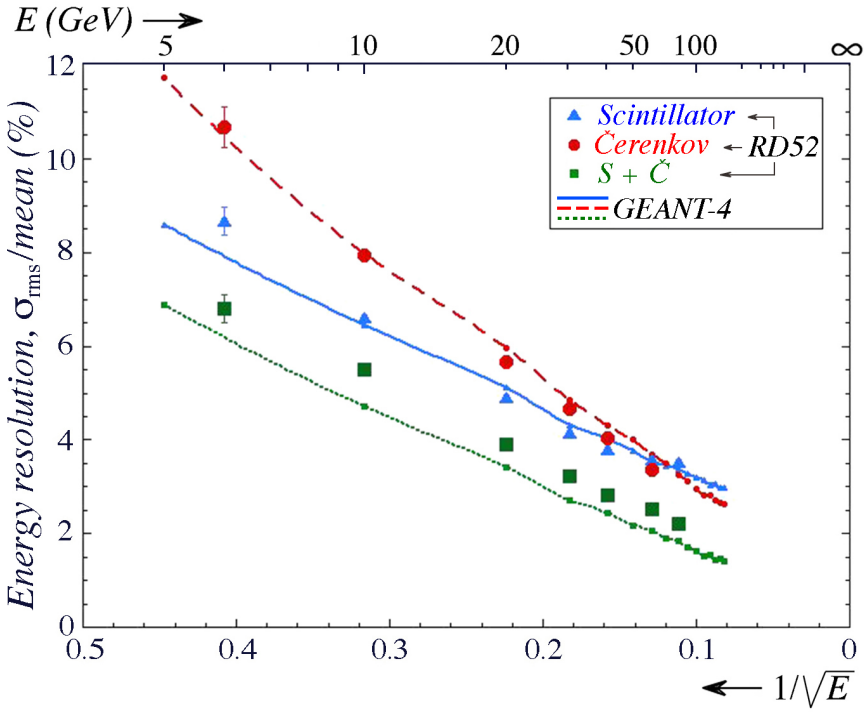

Fig. 14. The measured energy resolutions for the different signals as a function of the energy for the RD52 copper calorimeter [16], together with the GEANT4 calculations. The angle of incidence was (1.0°,1.5°).

The horizontal scale in the figure has been drawn linear in $E^{-1/2}$. Therefore, if the resolution would be completely determined by Poisson fluctuations, the data would lie on a straight line through the bottom right corner. The figure shows that the scintillation data clearly deviate from such a straight line. As mentioned above, the impact point dependence contributes an energy independent term to the energy resolution, which may be estimated to be of the order of 2-3%. The Čerenkov data suggest that such a term contributes at maxiumum 1% to the energy resolution.

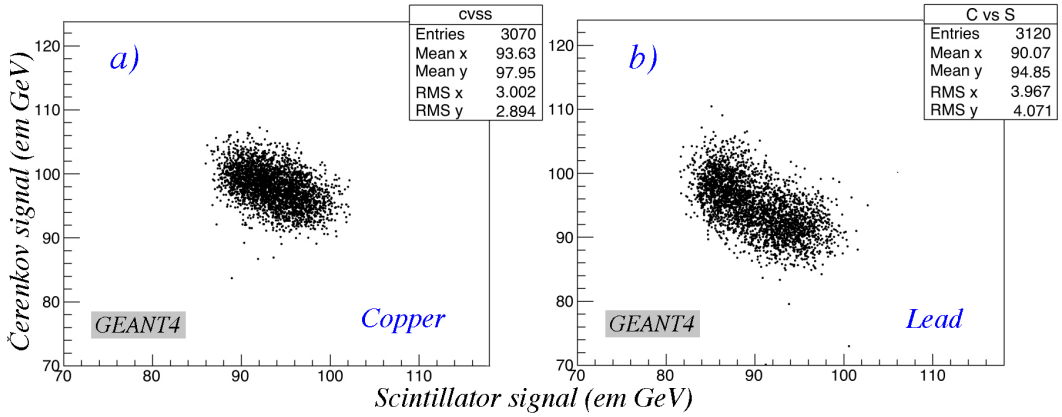

Fig. 15. Scatter plot of the Čerenkov versus the scintillation signals for 100 GeV electrons in the copper (a) and lead (b) calorimeter structures. Results from GEANT4 Monte Carlo simulations.

The figure also shows that the energy resolution for the sum of the scintillation and Čerenkov signals is somewhat smaller than observed in practice, although the energy dependence of this resolution is well described by the dotted (green) line. The predicted improvement in the energy resolution when combining both signals is somewhat surprising, since one would naively expect this improvement to be only due to the increased sampling fraction. Since the sampling fractions are identical for the copper/scintillator and copper/Čerenkov structures, one would expect the improvement in the resolution to be at best a factor of $\sqrt{2}$. At high energies, this is about the improvement experimentally observed. Yet, the improvement in the simulated energy resolution is clearly better. We investigated the reasons for this and found that there is an anti-correlation between the simulated scintillation and Čerenkov signals, as illustrated in Figure 15. Such an anti-correlation can be understood from the fact that the signals depend, on average, on the distance between the impact point and the nearest fiber that contributes to that signal, at least for the scintillation case (Figure 6). Apparently, this is also true for the Čerenkov signals and, therefore, adding both signals event by event leads to a substantial improvement in the energy resolution, since the effects responsible for a constant term in the resolution for the individual signals cancel each other. We checked if there was any evidence for this effect in the experimental data, but did not find any. For this reason, the experimental resolutions are a bit larger than the ones predicted by GEANT4.

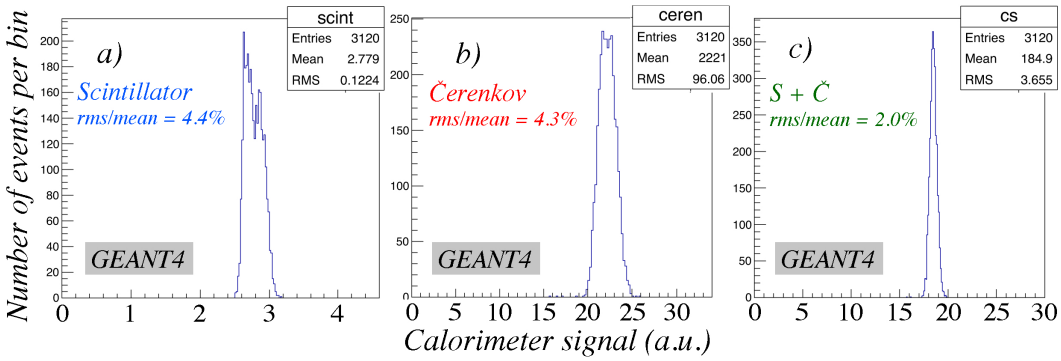

Fig. 16. The simulated response functions for 100 GeV electrons in the scintillation (a) and Čerenkov (b) channels, as well as the combined signal distribution (c), in the lead calorimeter. The electrons entered the detector at an angle (1.0°,1.5°).

Not surprisingly, the predicted improvement in the energy resolution resulting from combining the two signals is even more spectacular for the lead structure. This is because the impact point dependence of the response function and, therefore, the constant term in the energy resolution is significantly larger than in the case of copper, as illustrated by the *rms* values in Figure 15. At 100 GeV, elimination of this effect by combining the two signals is predicted to improve the resolution of the combined signal by more than a factor of two, compared to that for the individual signals. This is shown in Figure 16. Also in this case, no experimental evidence for this prediction was obtained. In fact, the measured resolution for the sum of both signals was only marginally better than that for the Čerenkov signal alone [16].

4.4.2 *Effects of an increase in the Čerenkov light yield*

Because of the good agreement between the simulated electromagnetic energy resolutions and the experimental data, it is also interesting to assess the improvement that might be expected if the light yield could be increased. This light yield is clearly a limiting factor for the resolution achievable in the Čerenkov channel. As indicated in the previous subsection, the simulations leading to the results shown in Figure 14 assumed a quantum efficiency for the detection of Čerenkov light of 0.11.

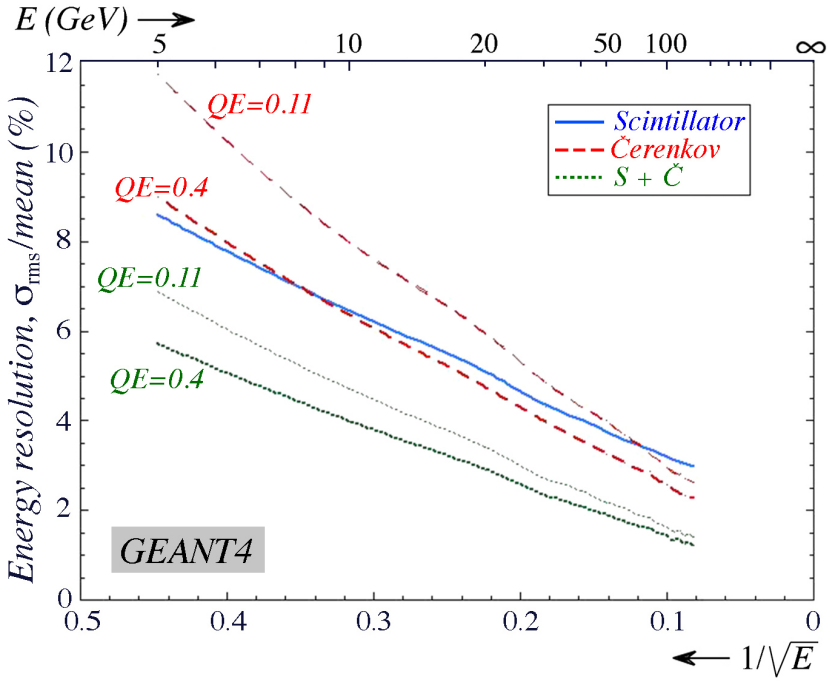

Fig. 17. The predicted effect of an increase in the Čerenkov light yield on the em energy resolution of the copper calorimeter. See text for details.

Figure 17 shows the effect of increasing this factor to 0.4 on the energy resolution in the Čerenkov channel and for the combined scintillator + Čerenkov signals. One consequence is that the Čerenkov resolution becomes better than the scintillation one for all energies greater than 10 GeV. Yet, the improvement of the energy resolution for the combined signals, which provides in practice by far the best resolution achievable for the detection of electromagnetic showers, is relatively modest: From 4.7% to 4.0% at 10 GeV and from 1.6% to 1.4% at 100 GeV.

5 Results for Hadrons

In the simulations of hadron showers, the emphasis was different than for the electromagnetic ones. A lack of (sufficiently detailed) experimental data was a major consideration in that respect. Our main goal was to investigate if and to what extent

the dual-readout method, which has been proven to work so nicely in practice, was as meritorious in the simulations. Important in that context is that the production of π^0s and other hadrons that develop em showers be correctly treated in the simulation of hadronic shower development. For meaningful comparisons with the experimental data, a correct description of the shower containment in the limited-volume detector is important too. The very-small-angle effects on the response function and the energy resolution that affected the em calorimeter performance play almost no role for hadronic showers, where typically hundreds (or more) fibers contribute significantly to the signals. On the other hand, saturation effects in the (scintillation) light production by densely ionizing particles are of great importance for hadron showers, while these effects are insignificant for em ones.

5.1 Hadronic response functions

Experimental data on the response of dual-readout calorimeters to hadrons are available for copper [8] and lead [18]. The hadronic response functions for 60 GeV pions in lead are shown in Figure 18. The experimental data are plotted in diagram a for the scintillation signals and in diagram b for the Čerenkov ones. The corresponding response functions predicted by GEANT4 are given in diagrams c (scintillation) and d (Čerenkov).

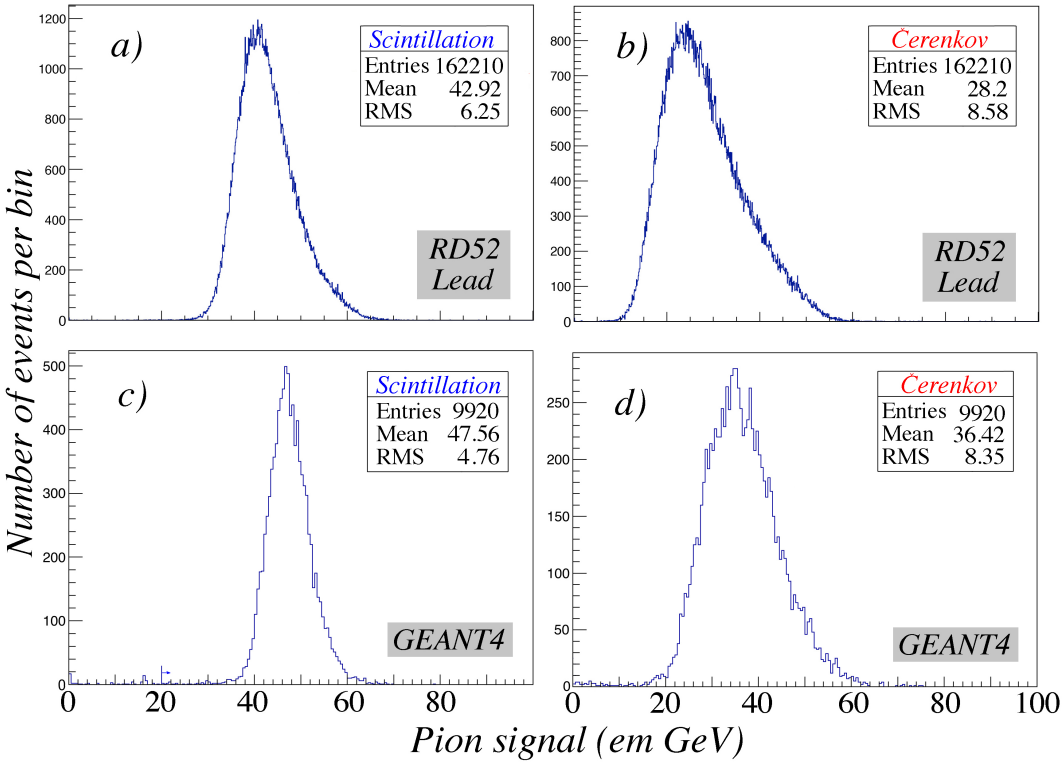

Fig. 18. The response functions for 60 GeV pions in the lead based RD52 calorimeter. Shown are the experimental data measured for the scintillation (a) and Čerenkov (b) signals, as well as the simulated response functions for these two types of signals (c, d).

The figure shows rather large discrepancies between the experimental data and the results of the simulations, both for the scintillation and the Čerenkov signals. In both cases, the mean value of the simulated response function was found to be quite a bit larger than the experimental value (48 *vs.* 43 GeV for the scintillation signals, 36 *vs.* 28 GeV for the Čerenkov ones). The characteristic asymmetric shape of the response function was somewhat better reproduced in the simulation of the Čerenkov signals, compared with the scintillation ones. The same was true for the *rms* widths of the signal distributions [6] .

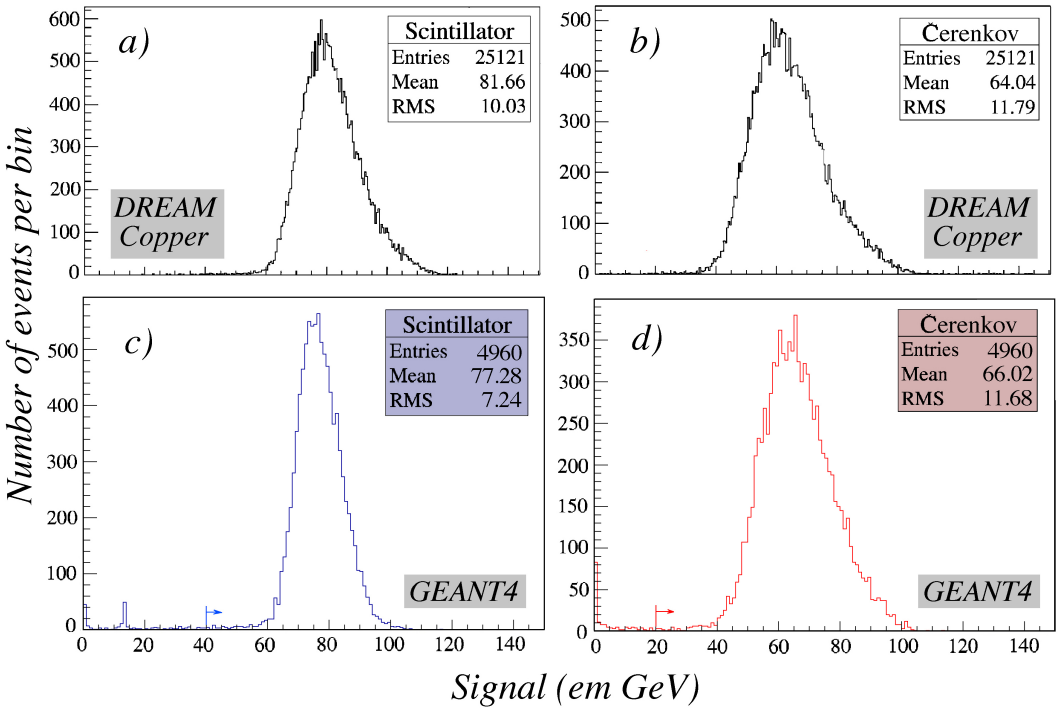

Fig. 19. The response functions for 100 GeV pions in the copper based DREAM calorimeter. Shown are the experimental data measured for the scintillation (a) and Čerenkov (b) signals [8], as well as the simulated response functions for these two types of signals (c, d).

The results of simulations of hadron showers in the copper based DREAM calorimeter were in better agreement with the experimental data. This is illustrated in Figure 19, which shows the response functions for 100 GeV pions. The experimental data are given in diagram a (scintillation) and in diagram b (Čerenkov). The corresponding results of the simulations are shown in diagram c (scintillation) and d (Čerenkov). The large discrepancy between the average signals in the experimental and simulated data for lead has largely disappeared and the shape and relative width of the simulated Čerenkov response function are in good agreement with the experimental results as well. However, the same cannot be said about the scintil-

[6] In order to make a more meaningful comparison with the experimental data, the *rms* values of the simulated distributions were determined for signals larger than a certain cutoff value, indicated by the arrows in Figures 18 and 19. The small signals were an artifact of the (0,0) angle of incidence, and disappeared completely for angles as small as 0.2°.

lation response function. Just as in the lead case, this response function is more symmetric and narrow than the measured one.

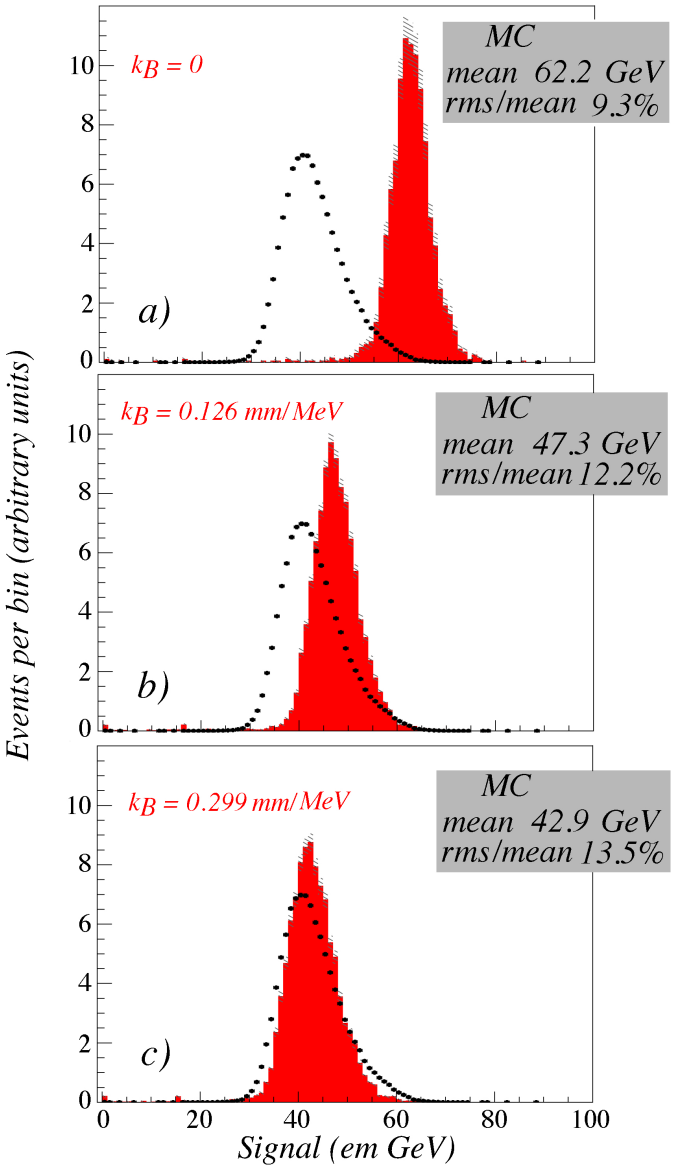

Fig. 20. Simulated scintillation signal distribution for 60 GeV pions in the RD52 lead calorimeter, without (a) or with (b, c) saturation effects for densely ionizing particles taken into account. The experimental data are shown for comparison. They are represented by the dots.

A major fraction of the non-em component of hadronic signals is caused by the numerous protons produced as a result of nuclear breakup reactions that take place in the shower development process. As described in Section 2.2, the signals from such protons (and from α particles and heavier nuclear aggregates) are subject to substantial saturation effects, described by Birks' constant (Equation 1). We verified that the large discrepancies observed between the simulated and experimental scintillation response functions, especially in the case of lead, were not caused by

a wrong parameterization of these saturation effects. To that end, we simulated 60 GeV pion showers with different values for Birks' constant:

- $k_B = 0$, *i.e.,* no saturation,
- $k_B = 0.126$ mm/MeV, *i.e.,* the established value for the type of scintillating fibers used in our detectors, and
- $k_B = 0.299$ mm/MeV, a value chosen because the average scintillation response equals that of the experimental distribution in that case.

Figure 20 shows the simulated response functions for these three values. Saturation clearly affects the scintillation response function. The larger Birks' constant, the smaller the calorimeter response. The response function also becomes more asymmetric, thus better resembling the experimental data. However, as one should expect, the value of k_B barely affects the Čerenkov response function. The copper based calorimeter used exactly the same type of scintillating fibers as the lead module. Figure 19 shows that the scintillation response for this calorimeter is *smaller* than the experimental value. Increasing the k_B value would further increase this discrepancy. Therefore, we don't see a compelling reason for concluding that the literature value of the k_B value, used in our simulations, is too small.

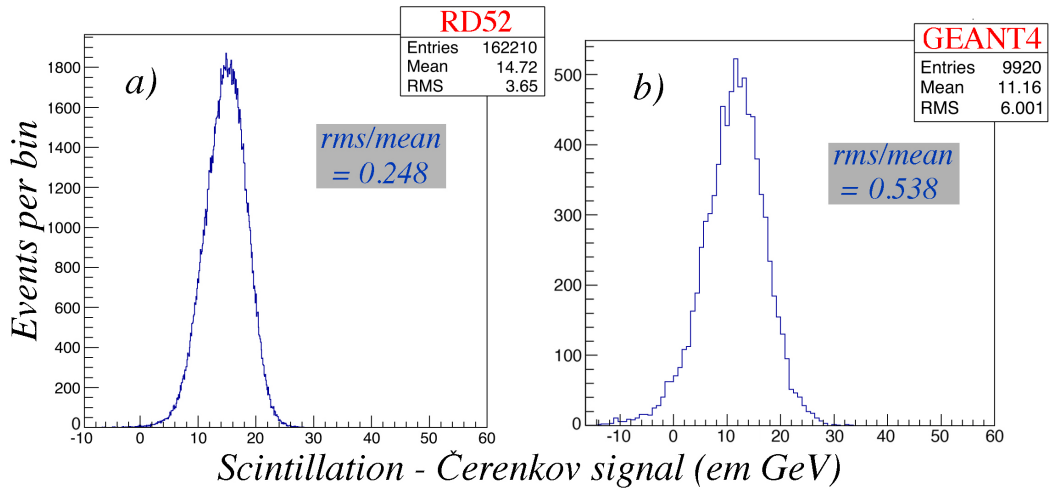

Fig. 21. Distribution of the event-by-event difference between the scintillation and Čerenkov signals for 60 GeV pions showering in the RD52 lead calorimeter. Shown are the experimental data (a) and the results of GEANT4 simulations of this process (b).

Another argument against an increased k_B value derives from considerations involving the event-to-event distribution of the *difference* between the scintillation and Čerenkov signals ($S - C$). For muons, $S - C$ reveals the contribution of the ionization component to the signals (see Figure 3). For hadron showers, $S - C$ is indicative for the distribution of the contribution of the non-relativistic shower component to the signals. Figure 21 shows the $S - C$ distributions for the experimental and simulated lead data. The mean value of the simulated distribution (11.2 GeV) is smaller than for the experimental data (14.7 GeV). Increasing the k_B value in the simulations would further increase this discrepancy. This is *a fortiori* true for

the signals from the copper calorimeter, where the difference between the average values of the simulated $S - C$ distribution (11.3 GeV) and the experimental data (17.6 GeV) is even larger than for lead.

Figure 21 also shows that the experimental distribution is more narrow and symmetric than the simulated one. These features indicate that the source of the observed discrepancies is the description of the "nuclear" processes, in which large numbers of non-relativistic protons and neutrons are produced, and which form the source of the *invisible energy*, *i.e.,* the nuclear binding energy which has to be provided by the showering particle and which does not contribute to any signal.

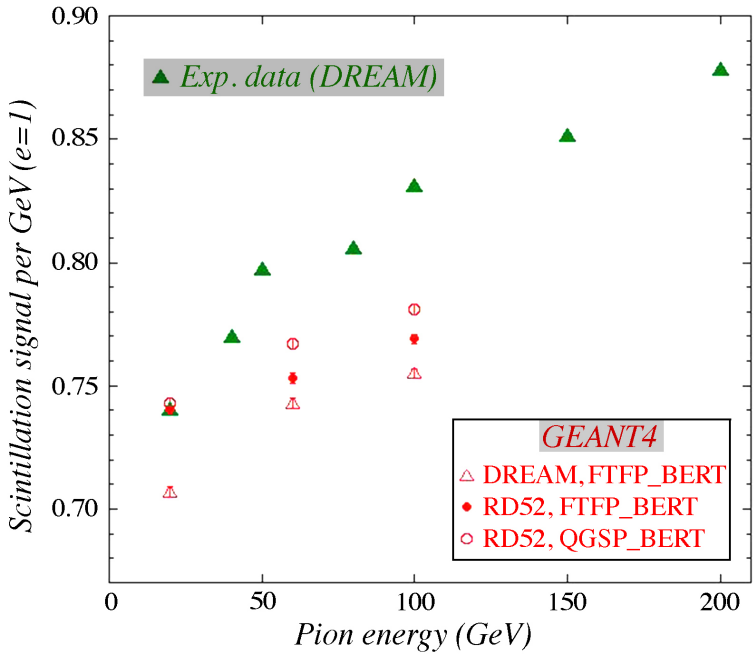

Fig. 22. The scintillation response to pions as a function of energy. The average scintillation signal per GeV is shown for the experimental data obtained with the DREAM calorimeter [8] and for various GEANT4 Monte Carlo simulations for copper (see appendix for details).

Additional evidence in support of this conclusion may be derived from the non-linearity of the calorimeter response to pions. Experimentally, the average scintillation signal per unit energy was observed to increase by about 12% between 20 and 100 GeV in the DREAM calorimeter (Figure 22). However, according to the GEANT4 simulations, the increase is considerably smaller (see the appendix for numerical details). Such a discrepancy was absent for the response of the calorimeter to the Čerenkov signals. Both for the lead and copper structures, GEANT4 predicts an increase of about 10% for the average signal from 60 GeV pions, compared to that for 20 GeV ones. This is in good agreement with the experimental observations. Since the Čerenkov signals are overwhelmingly caused by the em component of the hadron showers, *i.e.,* the π^0 component, we conclude from these comparisons that this component, and in particular its event-to-event fluctuations, are relatively well described in the simulation code.

5.2 *The dual-readout reconstruction of the energy*

The scintillation and Čerenkov signals simulated by GEANT4 were used to test the dual-readout method that has proven to be so successful with experimental data.

Figure 23 shows scatter plots in which each dot represents the scintillation and Čerenkov signals for a given event. These simulated data concern 100 (a), 60 (b) and 20 (c) GeV pions developing showers in the copper based dual-readout calorimeter. These data were used to reconstruct the energy of the showering particles, using [19,20]

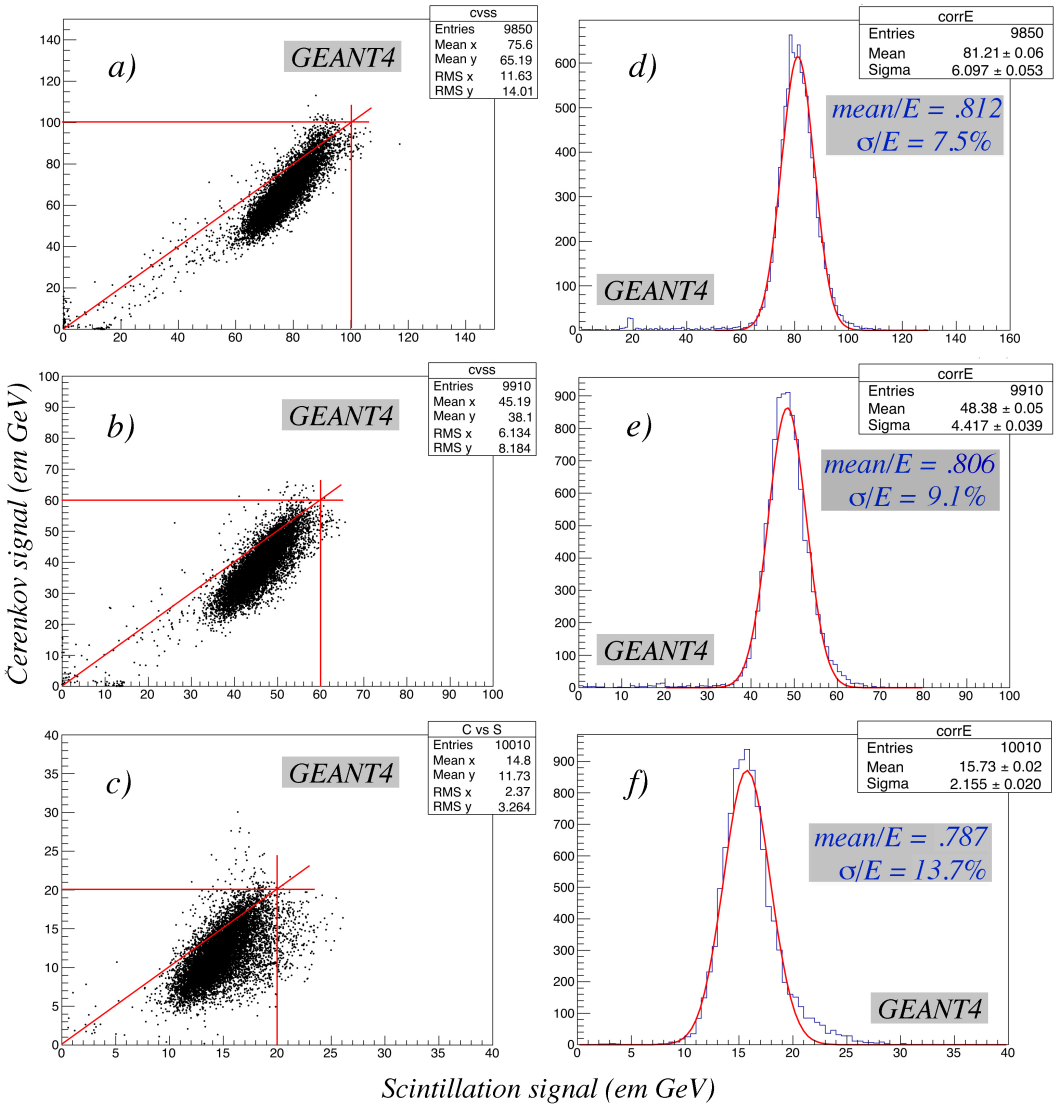

Fig. 23. Scatter plots of the Čerenkov *vs.* the scintillation signals for 100 GeV (a), 60 (b) and 20 GeV (c) pion showers in the copper based dual-readout fiber calorimeter, together with the reconstructed signal distributions derived from these scatter plots (d, e, f). Results from GEANT4 Monte Carlo simulations.

$$E = \frac{S - \chi C}{1 - \chi}, \quad \text{with } \chi = \frac{1 - (h/e)_S}{1 - (h/e)_C}. \tag{2}$$

The parameter χ is determined by the e/h values of the scintillation and Čerenkov fiber calorimeter structures. These values were measured to be 4.7 and 1.3 for the DREAM calorimeter [8], which leads to $\chi = 0.29$. This parameter value was used to reconstruct the observed energy distribution based on the simulated response functions for the scintillation and Čerenkov light. The results of this exercise are shown in Figures $23d$ (100 GeV), $23e$ (60 GeV) and $23f$ (20 GeV).

Especially at large energies, the distributions obtained in this way are much better described by a Gaussian function than the individual scintillation and Čerenkov response functions (see Figure 19). This confirms the experimental observations [8]. Also the energy resolutions obtained in this way are not too different from the experimental values. For example, at 100 GeV, the GEANT4 simulations for copper give a resolution of 7.5%, while the experimental value was measured to be 8.2% for pions developing showers in the calorimeter and 7.0% for pions interacting in a target just upstream of the calorimeter.

Yet, in one aspect, GEANT4 is clearly off, namely the fact that the average value of the E distribution is clearly too low. For fully contained showers, Equation 2 should reproduce the beam energy, and given the fact that the average side leakage is about 10% in this calorimeter, one should expect an average value around 90% of the beam energy. Yet, the simulations give typically only 80% (Figure $23d, e, f$). This is obviously a consequence of the fact that the scintillation response was typically too small and the Čerenkov response somewhat too large (Figure 19). Also, the linearity of the reconstructed energy (E) was not as good as for the experimental data. In the energy range from 20 - 100 GeV, the average E value per GeV increased by 2.4% in copper. This is a consequence of the discrepancies between the measured and calculated linearity of the scintillation response discussed in Section 5.1 (see Figure 22).

5.3 Radial profiles and shower containment

One of the reasons to embark on this study was to see to what extent the reconstruction of the hadron energy by means of the dual-readout method would benefit from enlarging the existing calorimeters. To that end, the structure simulated in GEANT4 (Figure 2) was enlarged to 7×7 modules, representing a lateral cross section of 65×65 cm^2. We used this structure to measure the radial shower profile, as well as the effects of enlarging the fiducial detector volume on the response functions and the reconstructed dual-readout energy.

Figure 24 shows the simulated radial profiles of 60 GeV pion showers developing in the copper (a) and lead (b) based fiber calorimeter structures. The energy mea-

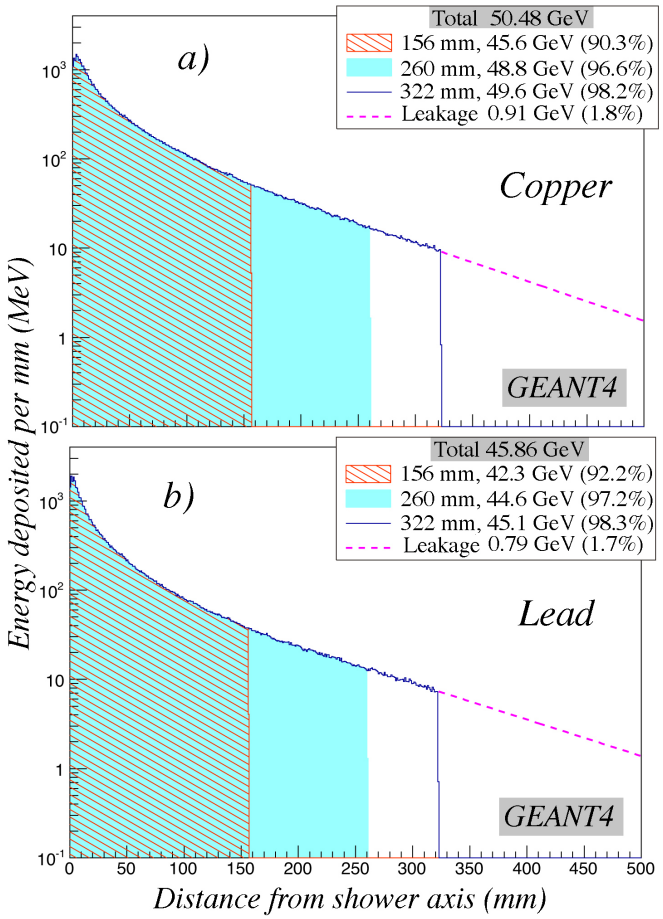

Fig. 24. Radial profiles for 60 GeV pions developing showers in the RD52 copper (a) or lead (b) based fiber calorimeters. Results from GEANT4 Monte Carlo simulations.

sured in thin cylindrical rings with a thickness of 1 mm is plotted as a function of their radius, *i.e.,* the distance from the shower axis. The legends show the total energy deposited in a 3×3, 5×5 and 7×7 module structure with the impact point in its center (see Figures 1, 2). They also show that the total measured energy does not equal the beam energy. This is a consequence of "invisible energy", in the form of lost nuclear binding energy, and neutrons, neutrinos and muons escaping from the detector. These losses are substantially larger in the case of a lead absorber. If we limit the analysis to the shower particles that do contribute to the calorimeter signal, we see that the energy leaking out of the experimentally tested (3×3) calorimeters amounts to 9.7% in the case of copper and 7.8% in the case of lead, in good agreement with the measured characteristics.

These simulation data were also used to evaluate to what extent the hadronic energy resolution would improve if the calorimeter would be enlarged to a 5×5 or 7×7 structure. The results, depicted in Figure 25, suggest a substantial improvement, especially at high energy, where the contributions of stochastic fluctuations to the energy resolution are so small that the resolution of the 3×3 calorimeter is dominated by fluctuations in shower leakage. For example, for 100 GeV pion show-

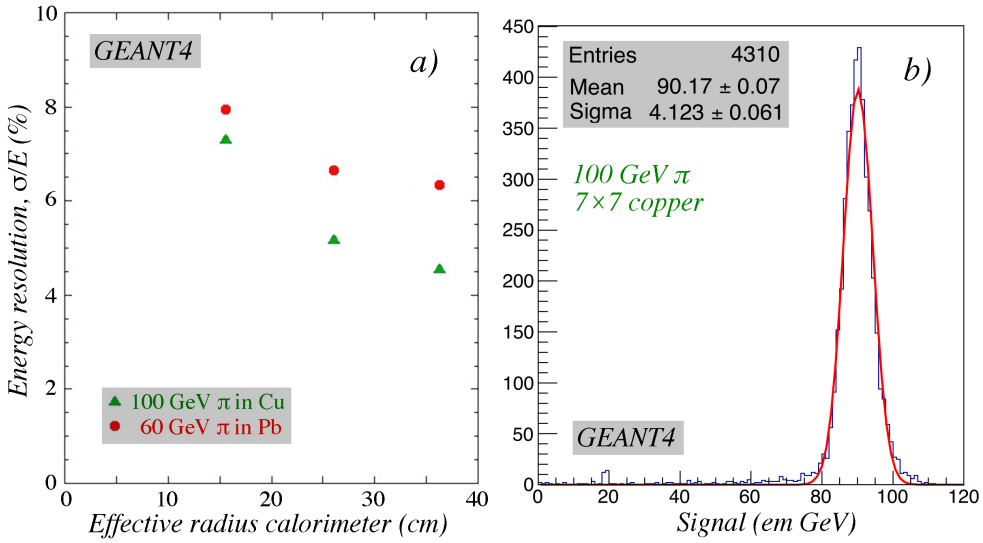

Fig. 25. The energy resolutions for 100 GeV and 60 GeV pions in dual-readout fiber calorimeters based on copper or lead absorber, respectively, as a function of the radial size of these calorimeters (a). The reconstructed energy distribution for 100 GeV pions in a 7×7 module dual-readout copper-fiber calorimeter (b). Results of GEANT4 Monte Carlo simulations.

ers in the copper calorimeter, the resolution is predicted to decrease from 7.5% in the 3×3 calorimeter to 5.2% in the 5×5 structure. A further increase to 7×7 modules would improve this resolution to 4.5%. According to Figure 24, the average shower leakage (at 60 GeV) decreases from 9.7% (3×3) to 3.4% (5×5) to 1.8% (7×7) as a result of such an increase of the instrumented detector volume. Figure 25b reconfirms the earlier observation (Figure 23) that the energy reconstruction based on the dual-readout formula (Equation 2) yields a value that is too low by $\sim 10\%$.

6 Discussion

The GEANT4 simulation package is the most widely used one in particle physics experiments, and is usually attributed great authority. However, as we have learned from the program of tests described in this paper, it clearly has its limitations, at least if one accepts that experimentally measured data represent a higher level of reality. To our knowledge, this is the first simulation of the performance of a fiber calorimeter based on the detection of Čerenkov light (or at least one of which the results are made public). The following is a summary of what we have learned from the Monte Carlo simulations of the performance of dual-readout fiber calorimeters.

- The simulation of the electromagnetic performance of the RD52 dual-readout calorimeters gave in general rather good results. Especially the scintillation signals were quite well reproduced. We refer in this context to the energy dependence

of the muon signals (Figure 3), the energy dependence of the energy resolution for electrons in the copper calorimeter (Figure 14), the shower profiles and the related shower containment results (Section 4.3).

- Some aspects of the Čerenkov signals were also quite well reproduced by the simulations. For example, at small angles of incidence the large difference between the shape of the em response functions for the two types of signals confirmed the experimentally observed reality (Figure 9). The same is true for the related fact that at high energies, the energy resolution is actually better when measured in the Čerenkov channel than in the scintillation one (Figure 14).
- Yet, when looking in more detail, we also found simulation results that were clearly at variance with the measured reality. The difference between the simulated scintillation and Čerenkov signals for muons was significantly smaller than measured, while the simulated Čerenkov signals were systematically too large (Figures 3,4). Another simulation result that is in disagreement with the experimental data concerns the energy resolution achievable for the combined scintillation + Čerenkov signals (Figures 14,16). Despite the fact that the predicted resolutions for the individual signals are in good agreement with the measured ones, the combined resolution is in practice not as good as suggested by the simulations. We have concluded that this discrepancy is the result of a perceived anti-correlation between the two types of signals which is in practice *not* observed (Figure 15). It is quite possible that at least some of these discrepancies are the result of a mistreatment of the requirement that the Čerenkov light has to be trapped within the numerical aperture of the fibers in order to contribute to the signals.
- One interesting, and for us somewhat unexpected, result of the simulations is the advantage of copper as an absorber material, compared to lead, even for electromagnetic showers. The advantage is particularly evident for particles entering the calorimeter at very small angles with the fiber direction. In copper, the degradation of the performance is already insignificant for angles as small as 0.2° (Figure 7), while the effects in lead are still noticeable at 2-3° (Figure 8). We have learned from these simulations that the orgin of this difference is the fact that the radiation length of copper is almost three times larger than for lead, while the Moliere radii (which govern the radial shower development) are about the same.
- Concerning hadronic shower development, the properties of the Čerenkov component are better reproduced by GEANT4 than the scintillation component. We have established that the non-relativistic component of the shower development, which is completely dominated by processes at the nuclear level, is rather poorly described by GEANT4. Both the average size of this component, as well as its event-to-event fluctuations are at variance with the experimental data. This manifests itself in the shape of the simulated scintillation response function, which is too narrow and less asymmetric than the experimentally measured one (Figures 18,19), and in the average contribution of the non-relativistic shower component to the calorimeter signals (Figure 21). The non-linearity of the calorimeter for hadronic signals is not well described for the scintillation signals (Figure 22).

Also in this respect, the agreement with the experimental data is better for the Čerenkov signals.

- Yet, some aspects of hadronic shower development that are important for the dual-readout application are in good agreement with the experimental data. As examples, we mention the shape of the Čerenkov response function and the radial shower profiles. Attempts to use the dual-readout technique on simulated shower data reasonably reproduced some of the essential characteristics and advantages of this method: A Gaussian response function, hadronic signal linearity and improved hadronic energy resolution. The fact that the reconstructed beam energy is systematically too low may be ascribed to the problems with the non-relativistic shower component mentioned above.
- For these reasons, we believe that the predicted improvement in the performance resulting from an increased detector size is realistic. The resolution of the instruments tested so far was clearly dominated by leakage fluctuations. An increase in the detector volume would reduce the effects of this, in which case resolutions of a few percent seem to be feasible.

Acknowledgments

This study was carried out with financial support of the United States Department of Energy, under contract DE-FG02-12ER41783, and by Italy's Istituto Nazionale di Fisica Nucleare and Ministero dell'Istruzione, dell'Università e della Ricerca. We gratefully acknowledge the facilities of and the support received from the High Performance Computing Center at Texas Tech University, where most of the (highly time consuming) simulations described in this paper were performed.

References

[1] R. Wigmans, Nucl. Instr. and Meth. **A732** (2013) 475, and references therein.
A complete list of DREAM and RD52 publications can be found at:
http://highenergy.phys.ttu.edu/dream/results/publications/publications.html

[2] S. Agostinelli *et al.*, Nucl. Instr. and Meth. **A506** (2003) 250.

[3] B. Andersson *et al.*, Nucl. Phys. **B281** (1987) 289.

[4] D. Wright *et al.*, AIP Conf. Proc. **896** (2006) 11.

[5] http://geant4.cern.ch/support/proc_mod_catalog/physics_lists/useCases.shtml

[6] J.B. Birks (1964), *The Theory and Practice of Scintillation Counting*, Oxford: Pergamon.

[7] R.L. Craun and D.L. Smith, Nucl. Instr. and Meth. **80** (1970) 239.

[8] N. Akchurin *et al.*, Nucl. Instr. and Meth. **A537** (2005) 537.

[9] N. Akchurin *et al.*, Nucl. Instr. and Meth. **A533** (2004) 305.

[10] K. Pinkau, Phys. Rev. **139B** (1965) 1548.

[11] U. Amaldi, Phys. Scripta **23** (1981) 409.

[12] C. Fabjan and T. Ludlam T, Ann. Rev. Nucl. Part. Sci. **32** (1982) 335.

[13] R. Wigmans (2000), *Calorimetry, Energy Measurement in Particle Physics*, International Series of Monographs on Physics, Vol. 107, Oxford University Press.

[14] W. Flauger, Nucl. Instr. and Meth. **A241** (1985) 72.

[15] E. Bernardi *et al.*, Nucl. Instr. and Meth. **A262** (1987) 229.

[16] N. Akchurin *et al.*, Nucl. Instr. and Meth. **A735** (2014) 130.

[17] D. Acosta *et al.*, Nucl. Instr. and Meth. **A308** (1991) 481.

[18] R. Wigmans, Nucl. Instr. and Meth. **A732** (2013) 475.

[19] D.E. Groom, Nucl. Instr. and Meth. **A572** (2007) 633; *ibid* **A697** (2013) 84; **A705** (2013) 24.

[20] R. Wigmans, New Journal of Physics **10** (2008) 025003.

[21] N. Akchurin *et al.*, Nucl. Instr. and Meth. **A536** (2005) 29.

Appendix - Effects of changes in the simulated geometry

All simulations described in this paper were carried out for a calorimeter with a simplified structure, which was not exactly the same as for the detectors that collected the experimental data with which comparisons are being made. Especially in the DREAM calorimeter, the fiber arrangement was quite different (see Figure 1c), and the RD52 calorimeter contained air gaps which were not taken into account in the simulations.

We have investigated the possible effects of these differences by means of a subset of additional simulations, in which the geometry was modified such as to better describe the experimental reality. The results of this exercise, which can be subdivided into three parts, are described in this appendix.

(1) We first investigated the possible effects of the presence of air in the RD52 calorimeters (see Fig. 1a,b). To that end, we have simulated a geometry such as the one shown in Fig. 2c, but with each fiber surrounded by an air gap

with a thickness of 50 microns. The simulations with this structure were carried out with copper as absorber material. Since part of the copper is now replaced by air, the sampling fraction for *mip*s increases from 3.9% to 4.4%. This may be compared with the sampling fraction of the RD52 copper calorimeter, which was 4.6% or 4.3%, depending on whether the fiber cladding is considered part of the active material or not. Other than the (trivial) effects resulting from the small increase in the sampling fraction, this change in the geometry had no significant effects on the results of the simulations. Because of the increased sampling fraction, the signals were somewhat larger and the calibration constants correspondingly smaller. The em energy resolution was also somewhat better, because of the reduced contribution of sampling fluctuations. However, the characteristic effects described in this paper, such as the angular dependence of the response function and the differences in that respect between the scintillation and Čerenkov signals (Figs. 6 - 13), or the anti-correlation between these two types of signals (Figs. 15,16) were not affected by this change in geometry.

Some numerical information: The e/mip value was found to be 0.83 in this "air-gap geometry", versus 0.84 without the air-gap. The energy resolution for 40 GeV electrons (Fig. 14) improved from 4.03% to 3.43% as a result of the air-gap in the scintillation channel. The experimental RD52 value was 3.78$\pm$0.04%. For the Čerenkov channel, an improvement was observed from 4.32% to 3.96% (experimental value 4.09$\pm$0.04%). For the combined S+C signals the resolution improved from 2.44% to 2.32% as a result of the air gap. The fact that the experimental value (2.85$\pm$0.03%) for this sum was $\sim$ 20% larger than both these values is a consequence of the fact that the anti-correlation between the S and C signals (Figs. 16,17 with and without the air gap) was not observed in reality. In summary, we believe that the conclusions drawn on the basis of the original GEANT4 simulations for electrons remain valid after these checks.

(2) To check the validity of some of our conclusions, we have implemented the DREAM geometry (see fig. 1c) in our simulation code. This code was used to simulate the response to hadrons and muons in copper, since some of the experimental data with which comparisons were made (figs. 3,4,19,22) were obtained with the DREAM calorimeter. The simulations with this DREAM geometry were carried out for 20, 60 and 100 GeV pions in copper, and also for muons with energies between 10 and 200 GeV traversing the DREAM calorimeter at 6 degrees with the fiber direction. The results obtained for the hadrons remained significantly different from the experimental data, both in terms of the response functions (fig. 19) and the hadronic signal linearity (fig. 22). For example, the non-linearity of the scintillation signals between 20 and 100 GeV, which was measured to be 1.123$\pm$0.010, was found to be 1.068$\pm$0.010 in these simulations, and the ratio $\sigma_{\rm rms}$/mean for the scintillation signals from 100 GeV pions, which was measured to be (12.3$\pm$0.2)% turned out to be (10.3$\pm$0.3)% according to these simulations.

As in the RD52 geometry, the characteristics of the Cherenkov signals were

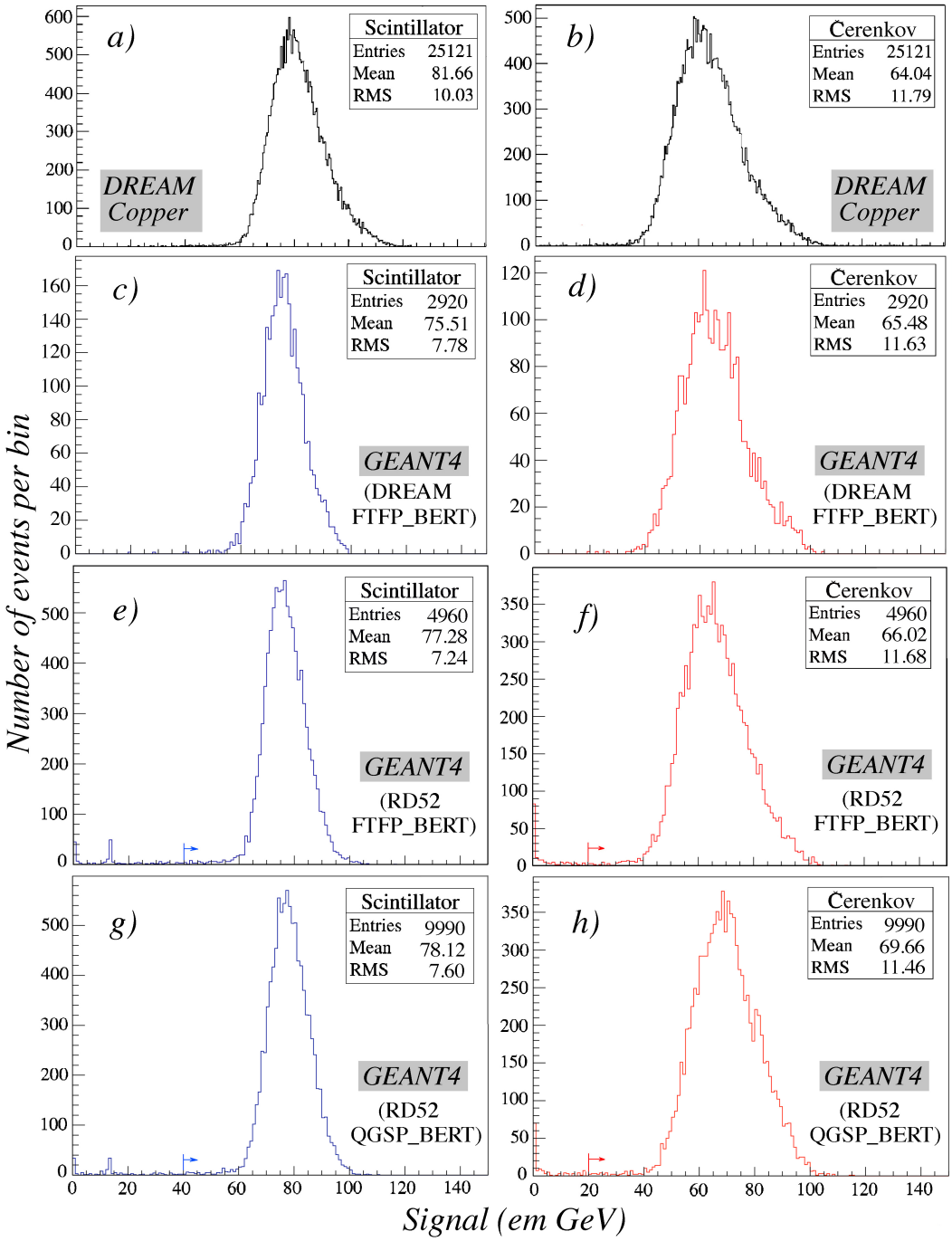

Fig. 26. The response functions for 100 GeV pions in the copper based DREAM calorimeter. Shown are the experimental data measured for the scintillation (a) and Čerenkov (b) signals [8], as well as the simulated response functions for these two types of signals in the DREAM geometry (c, d), in the RD52 geometry with the FTFP_BERT package (e, f) and in the RD52 geometry with the QGSP_BERT package (g, h).

better reproduced than those of the scintillation signals in the simulations with the DREAM geometry. For example, the energy resolution for 100 GeV pions ($\sigma_{\rm rms}$/mean) was found to be (17.8$\pm$0.5)% with the DREAM geometry, vs. (17.7$\pm$0.4)% with the RD52 geometry (FTFP_BERT) , while the measured value was (18.4$\pm$0.3)%. Also, the mean value of the Cherenkov signals was in better agreement with the experimental result (65.5 GeV for the DREAM simulations, 64.0 GeV measured) than for the scintillation signals (75.5 GeV for the DREAM simulations, 81.7 GeV measured).

For electron showers, where the number of fibers that contribute significantly to the signals is one to two orders smaller than for hadrons, the experimentally observed differences between the response functions for the two types of signals [21] were confirmed in the simulations with the DREAM geometry (As for all other simulations, 40 GeV electrons were used to determine the calibration constants).

The GEANT4 simulations of the signals from muons (to which even fewer fibers contributed) gave somewhat better agreement with the experimental data when the DREAM geometry was used, even though the essential features of the data were also reproduced for simulations with the RD52 geometry. This was in particular true for the increase of the signals with the muon energy and the fact that the scintillation signal was larger than the Čerenkov signal, by an energy independent amount (figure 3).

(3) We have also used the original (RD52) geometry for hadron simulations with a different hadron package implemented in GEANT4, QGSP_BERT. The simulations with the QGSP_BERT package were also carried out for 20, 60 and 100 GeV pions in copper (RD52 geometry). The differences with the results obtained with the FTFP_BERT package were minor and did not significantly improve the main discrepancies between experimental and simulated performance. For example, the distribution of the scintillation signal (fig. 20) was still more narrow and more symmetric than in reality. The ratio $\sigma_{\rm rms}$/mean for 100 GeV pions was found to be (9.4$\pm$0.3)% for FTFP_BERT, (9.7$\pm$0.3)% for QSGP_BERT, *vs.* (12.3$\pm$0.2)% in the experiment. The non-linearity between 20 and 100 GeV (*i.e.,* the ratio between the average signal per GeV at 100 and at 20 GeV, see fig. 22), which was measured to be 1.123$\pm$0.010, was simulated to be 1.039$\pm$0.008 with FTFP_BERT and 1.051$\pm$0.008 with QGSP_BERT. Figure 26 summarizes the results obtained for the different simulations of 100 GeV π^- showers, and the non-linearity of the hadronic scintillation signals obtained with the different simulations is shown in Figure 22.

In summary, we believe that the conclusions drawn on the basis of the original hadron simulations remain valid after these checks.

List of Figures

26 The response functions for 100 GeV pions in the copper based DREAM calorimeter. Shown are the experimental data measured for the scintillation (a) and Čerenkov (b) signals [8], as well as the simulated response functions for these two types of signals in the DREAM geometry (c, d), in the RD52 geometry with the FTFP_BERT package (e, f) and in the RD52 geometry with the QGSP_BERT package (g, h). 35